Synthesis and Reactivity of Heterobimetallic "A-Frames" and Rh–Zr Bonded Complexes: Structure of $Cp^*Zr(\mu\text{-}OCH_2Ph_2P)_2RhMe_2$

Gregory S. Ferguson, Peter T. Wolczanski,*,† László Párkányi,‡ and Marjanne C. Zonnevylle

Department of Chemistry, Baker Laboratory, Cornell University, Ithaca, New York 14853

Received December 8, 1987

The preparations of Rh/Zr "A-frame" and metal–metal bonded complexes are detailed. Treatment of $Cp^*MeZr(OCH_2Ph_2P)_2$ (**2**, $Cp^* = \eta^5\text{-}C_5Me_5$), prepared from Cp^*ZrMe_3 (**1**) and $2.0HOCH_2Ph_2P$, with $0.5[(OC)_2RhCl]_2$ (**3**) afforded $Cp^*Zr(\mu\text{-}OCH_2Ph_2P)_2(\mu_2\text{-}\eta^2\text{-}O{=}C(CH_3))(\mu\text{-}Cl)RhCO$ (**4**). The $\mu_2\text{-}\eta^2$-acetyl bridge was cleaved from **4** by HCl to yield acetaldehyde (61%) and $Cp^*Zr(\mu\text{-}OCH_2Ph_2P)_2(\mu\text{-}Cl)_2RhCO$ (**5**, 68%), more conveniently isolable from refluxing **4** in $CHCl_3$. ^1H NMR and IR evidence for an acetyl–hydride intermediate, $[Cp^*Zr(\mu\text{-}OCH_2Ph_2P)_2(\mu_2\text{-}\eta^2\text{-}O{=}C(CH_3))(\mu\text{-}Cl)Rh(CO)H]Cl$ (**[4H]Cl**), was obtained. Acetone (93%) and $Cp^*Zr(\mu\text{-}OCH_2Ph_2P)_2(\mu\text{-}Cl)(\mu\text{-}I)RhCO$ (**7**, 85%) are formed from exposure of **4** to MeI. The reaction of $(Ph_3P)_3RhMe$ (**8a**) with **2** provided $Cp^*Zr(\mu\text{-}OCH_2Ph_2P)_2RhMe_2$ (**9**), which contains a short 2.444 (1) Å Rh–Zr bond generated via the oxidative addition of a ZrMe group to Rh. Crystal data: triclinic, $P\bar{1}$, a = 11.734 (1) Å, b = 10.524 (1) Å, c = 15.266 (1) Å, α = 104.15 (1)°, β = 93.92 (2)°, and γ = 112.90 (2)°, Z = 2, T = 25 °C, R = 0.063, R_w = 0.051 (2717 (60.2%) reflections where $|F_o| \geq 3\sigma(F_o)$). Byproduct $Cp^*Zr(\mu\text{-}OCH_2Ph_2P)_3RhMe$ (**11**) was best synthesized through the addition of $Cp^*Zr(OCH_2Ph_2P)_3$ (**10**) to **8a**. Through a similar pathway, $(Ph_3P)_3RhH$ (**8b**) and **2** yielded $Cp^*Zr(\mu\text{-}OCH_2Ph_2P)_2RhPPh_3$ (**12**) concomitant with $0.96CH_4$. Hydrogenation of **12** or **9** ($-1.9CH_4$) produced $Cp^*Zr(\mu\text{-}OCH_2Ph_2P)_2RhH_2(PPh_3)$ (**13**). The latter hydrogenated C_2H_4 to give ethane and **12** or $Cp^*Zr(\mu\text{-}OCH_2Ph_2P)_2Rh(\eta^2\text{-}C_2H_4)$ (**14**), if excess was used. The reversible binding of PPh_3 to **13** and **14** was evidenced. Extended Hückel calculations performed on a model of **9** revealed that the Rh–Zr interaction is 47% σ and 53% π in character, providing a strong indication of multiple bonding. Alternatively, **9** may be considered a donor/acceptor complex with Zr acting as a σ- and π-acceptor Lewis acid. The results were compared with calculations addressing similar M–M′ bonded systems. The relationship of the compounds above to heterogeneous oxygenate-selective F–T catalysts and strong metal-support interactions (SMSI) is also discussed.

Introduction

Organometallic species have proven valuable in modeling the reactivity and spectroscopic properties of catalytically active heterogeneous surfaces.[1,2] Homogeneous investigations have focused on transformations that make and break C–C and C–O bonds, especially those which probe the Fischer–Tropsch (F–T) reaction sequence.[3] Recently, numerous heterobimetallic complexes have been prepared;[4] the combination of early and late metals[5] is particularly relevant to the aforementioned heterogeneous materials, since these are usually comprised of electron-rich metals deposited on a Lewis acidic metal oxide support. The latter cocatalyst undoubtedly serves as a dispersive medium, yet in many instances extensive involvement in the surface chemistry is evident.[6,7] Strong metal-support interactions (SMSI)[8,9] of late metal/early metal oxide catalysts suggest that the components function in a cooperative manner at their interface, where small molecule reactivity may occur.

In this laboratory,[10–12] the heterogeneous interface has been modeled by constructing complexes in which early and late metal centers are linked via an alkoxyalkylphosphine[13] bridge. The alkoxide end of $\mu\text{-}OCH_2Ph_2P$, when linked to an early metal, serves to model the $[MO_n]_m$ component;[14,15] the softer phosphine segment binds to low-valent late metals, representing an electron-rich surface. Alkyl migrations across the homogeneous interface depicted (I) have been observed through methyl scrambling reactions of $Cp^*ZrMe(\mu\text{-}OCH_2Ph_2P)_2PtMe_2$.[12] As noted in a preliminary communication, the formation and subsequent chemistry of $Cp^*Zr(\mu\text{-}OCH_2Ph_2P)_2(\mu_2\text{-}\eta^2\text{-}O{=}CMe)(\mu\text{-}Cl)RhCO$ involves both metal centers,[11] implicating a similar cooperation between the components of

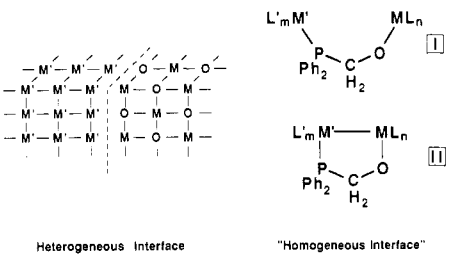

† Alfred P. Sloan Foundation Fellow (1987–1989).

‡ On leave from the Central Research Institute of Chemistry, Hungarian Academy of Science, Budapest, Hungary.

(1) (a) Bradley, J. S. *Adv. Organomet. Chem.* **1983**, *22*, 1–58. (b) Gladysz, J. A. *Ibid.* **1982**, *20*, 1–38. (c) Herrmann, W. A. *Ibid.* **1982**, *20*, 159–263. (d) Herrmann, W. A. *Angew. Chem., Int. Ed. Engl.* **1982**, *21*, 117–130. (e) Muetterties, E. L.; Stein, J. *Chem. Rev.* **1979**, *79*, 479–490. (f) Muetterties, E. L.; Rhodin, T. N.; Band, E.; Brucker, C. F.; Pretzer, W. R. *Ibid.* **1979**, *79*, 91–137. (g) Tachikawa, M.; Muetterties, E. L. *Prog. Inorg. Chem.* **1981**, *28*, 203–238. (h) Erker, G. *Acc. Chem. Res.* **1984**, *17*, 103–109. (i) Wolczanski, P. T.; Bercaw, J. E. *Ibid.* **1980**, *13*, 121–127. (j) Floriani, C. *Pure Appl. Chem.* **1983**, *55*, 1–10. (k) Horwitz, C. P.; Shriver, D. F. *Adv. Organomet. Chem.* **1984**, *23*, 219–305.

(2) For some pertinent recent articles, see: (a) Erker, G.; Dorf, U.; Atwood, J. L.; Hunter, W. E. *J. Am. Chem. Soc.* **1986**, *108*, 2251–2257. (b) Gambarotta, S.; Floriani, C.; Chiesi-Villa, A.; Guastini, C. *Organometallics* **1986**, *5*, 2425–2433. (c) Roddick, D. M.; Fryzuk, M. D.; Seidler, P. F.; Hillhouse, G. L.; Bercaw, J. E. *Ibid.* **1985**, *4*, 97–104. (d) Barger, P. T.; Santarsiero, B. D.; Armantrout, J.; Bercaw, J. E. *J. Am. Chem. Soc.* **1984**, *106*, 5178–5186. (e) Moloy, K. G.; Marks, T. J. *Ibid.* **1984**, *106*, 7051–7064. (f) Wayland, B. B.; Woods, B. Z.; Pierce, R. *Ibid.* **1982**, *104*, 302–303. (g) Paonessa, R. S.; Thomas, N. C.; Halpern, J. *Ibid.* **1985**, *107*, 4333–4335. (h) Belmonte, P. A.; Cloke, F. G. N.; Schrock, R. R. *Ibid.* **1983**, *105*, 2643–2650. (i) Hriljac, J. A.; Shriver, D. F. *Ibid.* **1987**, *109*, 6010–6015.

(3) (a) Falbe, J. *Chemical Feedstocks from Coal*; Wiley: New York, 1981. (b) Bell, A. T. *Catal. Rev.—Sci. Eng.* **1981**, *23*, 203–232. (c) Biloen, P.; Sachtler, W. M. H. *Adv. Catal.* **1981**, *30*, 165–216. (d) Rofer-DePoorter, C. K. *Chem. Rev.* **1981**, *81*, 447–474.

(4) (a) Roberts, D. A.; Geoffrey, G. L. *Comprehensive Organometallic Chemistry*; Wilkinson, G., Stone, F. G. A., Abel, E. W., Eds.; Pergamon: Oxford, 1982; Chapter 40. (b) Bruce, M. I. *J. Organomet. Chem.* **1985**, *283*, 339–414.

0276-7333/88/2307-1967$01.50/0

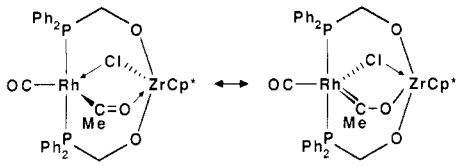

Figure 1.

heterogeneous Rh/ZrO_2,[16] an oxygenate-selective[17-19] F-T catalyst. The full details of the latter investigation are described in this paper.

In the previous studies,[10-12] the interaction between M′ and M (M = early, M′ = late) was either nonexistent (I) or at most weakly dative (M′→M). Through pioneering efforts by Casey et al.,[5,20] approaches to activating small molecules (e.g. H_2, CO) by exploiting the polarity of the early/late M–M′ single bond have been explored. The chemistry of $Cp_2Zr\{Ru(CO)_2Cp\}_2$ has culminated in the reduction of CO in a bifunctional, albeit unusual fashion.[20] Presented herein are complexes containing formal Rh–Zr single bonds (II), viewed above as an alternate homogeneous interface. Extended Hückel (EH) calculations are utilized to examine the nature of various bimetallic interactions, and the possible relevance of M–M′ bonding to SMSI is discussed.

Results and Discussion

μ_2-η^2-Acetyl-Rh/Zr Synthesis. The formation of μ-

Scheme I

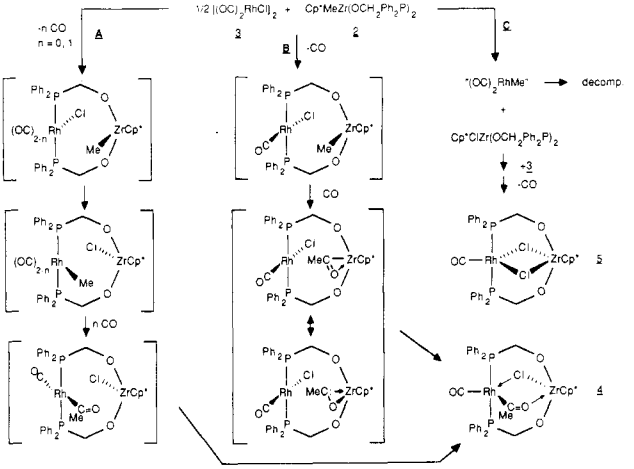

OCH_2Ph_2P bridges linking Zr and Rh was accomplished via alcoholysis at the early metal followed by substitution at the late metal center. Treatment of Cp^*ZrMe_3 (**1**, $Cp^* = \eta^5$-C_5Me_5)[21] with 2 equiv of $HOCH_2Ph_2P$[13] produced $Cp^*MeZr(OCH_2Ph_2P)_2$ according to eq 1. Typically

$$\underset{\mathbf{1}}{Cp^*ZrMe_3} + 2HOCH_2Ph_2P \xrightarrow[\text{hexane, 25 °C}]{-2CH_4} \underset{\mathbf{2}}{Cp^*MeZr(OCH_2Ph_2P)_2} \quad (1)$$

produced as a clear oil of purity >90%, **2** could be induced to precipitate from hydrocarbon solutions by exposure to trace amounts of air. Precipitation resulted in analytically pure microcrystalline material in 80–90% yields. From $^{31}P\{^1H\}$ NMR evidence, the phosphines are not chelated to Zr since their resonance at δ −11.24 is sharp and comparable to that of $HOCH_2Ph_2P$ (δ −11.84).

When 1.0 equiv of **2** was combined with $0.5[(OC)_2RhCl]_2$ (**3**)[22] in toluene at −78 °C and the mixture allowed to warm to room temperature, the μ_2-η^2-acetyl[20,23,24] "A-frame"[25] $Cp^*Zr(\mu\text{-}OCH_2Ph_2P)_2(\mu_2\text{-}\eta^2\text{-}O{=}C(CH_3))(\mu\text{-}Cl)RhCO$ (**4**) precipitated as yellow, microcrystalline flakes (eq 2, Figure 1). μ_2-η^2-Acetyl **4** was typically obtained in 45–65% isolated yield after the related dichloro-bridged species (vide infra) $Cp^*Zr(\mu\text{-}OCH_2Ph_2P)_2(\mu\text{-}Cl)_2RhCO$ (**5**), a persistent

$$\underset{\mathbf{2}}{2} + \tfrac{1}{2}\underset{\mathbf{3}}{[(OC)_2RhCl]_2} \xrightarrow[25\ °C]{\text{toluene}} \underset{\mathbf{4}\ (45\text{–}65\%)}{Cp^*Zr(\mu\text{-}OCH_2Ph_2P)_2(\mu_2\text{-}\eta^2\text{-}O{=}C(CH_3))(\mu\text{-}Cl)RhCO} + \underset{\mathbf{5}\ (5\text{–}10\%)}{Cp^*Zr(\mu\text{-}OCH_2Ph_2P)_2(\mu\text{-}Cl)_2RhCO} \quad (2)$$

(5) Casey, C. P.; Bullock, R. M. *Acc. Chem. Res.* **1987**, *20*, 167–173.
(6) Maier, W. F. *Nature (London)* **1987**, *329*, 531–534.
(7) (a) Mims, C. A.; McCandlish, L. E. *J. Phys. Chem.* **1987**, *91*, 929–937. (b) Zhang, X.; Biloen, P. *J. Catal.* **1986**, *98*, 468–476. (c) Vannice, M. A.; Sudhaker, C. *J. Phys. Chem.* **1984**, *88*, 2429–2432. (d) Mori, T.; Masuda, H.; Imai, H.; Taniguchi, S.; Miyamoto, A.; Hattori, T.; Murakami, Y. *J. Chem. Soc., Chem. Commun.* **1986**, *1244*–1245. (e) Biloen, P.; Helle, J. N.; van den Berg, F. G. A.; Sachtler, W. M. *J. Catal.* **1983**, *81*, 450–458. (f) Dauscher, A.; Garin, F.; Maine, G. *Ibid.* **1987**, *105*, 233–244.
(8) (a) Tauster, S. J. *Acc. Chem. Res.* **1987**, *20*, 389–394. (b) *Strong Metal-Support Interactions*; Baker, R. T. K., Tauster, S. J.; Dumesic, J. A., Eds.; ACS Symposium Series 298; American Chemical Society: Washington, DC, 1986. (c) *Metal-Support and Metal Additive Effects in Catalysis*; Imelik, B., et al., Eds.; Elsevier: Amsterdam, 1982. (d) Tauster, S. J.; Fung, S. C.; Baker, R. T. K.; Horsley, J. A. *Science (Washington, D.C.)* **1981**, *211*, 1121–1125.
(9) (a) Sanchez, M. G.; Gazquez, J. L. *J. Catal.* **1987**, *104*, 120–133. (b) Sadeghi, H. R.; Henrich, V. E. *Ibid.* **1988**, *109*, 1–11. (c) Resasco, D. E.; Weber, R. S.; Sakellson, S.; McMillan, M.; Haller, G. L. *J. Phys. Chem.* **1988**, *92*, 189–193.
(10) Ferguson, G. S.; Wolczanski, P. T. *Organometallics* **1985**, *4*, 1601–1605.
(11) Ferguson, G. S.; Wolczanski, P. T. *J. Am. Chem. Soc.* **1986**, *108*, 8293–8295.
(12) Baxter, S. M.; Ferguson, G. S.; Wolczanski, P. T. *J. Am. Chem. Soc.*, in press.
(13) Hellmann, von H.; Bader, J.; Brikner, H.; Schumacher, O. *Liebigs Ann. Chem.* **1962**, *659*, 49–63.
(14) (a) Chisholm, M. H.; Clark, D. L.; Huffman, J. C.; Smith, C. A. *Organometallics* **1987**, *6*, 1280–1291. (b) Chisholm, M. H.; Heppert, J. A.; Huffman, J. C.; Streib, W. E. *J. Chem. Soc., Chem. Commun.* **1985**, 1771–1773. (c) Chisholm, M. H. *Nouv. J. Chim.* **1987**, *11*, 459–465.
(15) (a) LaPointe, R. E.; Wolczanski, P. T.; Mitchell, J. F. *J. Am. Chem. Soc.* **1986**, *108*, 6382–6384. (b) Toreki, R.; LaPointe, R. E.; Wolczanski, P. T. *Ibid.* **1987**, *109*, 7558–7560.
(16) (a) Dall'Agnol, C.; Gervasini, A.; Morazzoni, F.; Pinna, F.; Strukul, G.; Zanderighi, L. *J. Catal.* **1985**, *96*, 106–114. (b) Ichikawa, M. *Bull. Chem. Soc. Jpn.* **1978**, *51*, 2273–2277.
(17) (a) Poels, E. K.; Ponec, V. *Catalysis*; Chemical Society: London, 1983; Specialist Periodic Reports, Vol. 6, p 196. (b) Dombek, B. D. *Adv. Catal.* **1983**, *32*, 325–416.
(18) (a) van der Lee, G.; Schuller, B.; Post, H.; Favre, T. L. F.; Ponec, V. *J. Catal.* **1986**, *98*, 522–529. (b) Takeuchi, A.; Katzer, J. R. *Ibid.* **1983**, *82*, 351–354. (c) Takeuchi, A.; Katzer, J. R. *J. Phys. Chem.* **1982**, *86*, 2438–2441. (d) Ichikawa, M.; Sekizawa, S.; Shikakura, K.; Kawai, M. *J. Mol. Catal.* **1981**, *11*, 167–179.
(19) (a) van der Lee, G.; Ponec, V. *J. Catal.* **1986**, *99*, 511–512. (b) Sachtler, W. M. H.; Shriver, D. F.; Ichikawa, M. *Ibid.* **1986**, *99*, 513–514.
(20) (a) Casey, C. P.; Palermo, R. E.; Rheingold, A. L. *J. Am. Chem. Soc.* **1986**, *108*, 549–550. (b) Casey, C. P.; Palermo, R. E.; Jordan, R. F.; Rheingold, A. L. *Ibid.* **1985**, *107*, 4597–4599 and references therein.
(21) Wolczanski, P. T.; Bercaw, J. E. *Organometallics* **1982**, *1*, 793–799.
(22) McCleverty, J. A.; Wilkinson, G. *Inorganic Syntheses*; Holtzclaw, H. F., Jr., Ed.; McGraw-Hill: New York, 1966; Vol. VIII, pp 211–214.
(23) Marsella, J. A.; Huffman, J. C.; Caulton, K. G.; Longato, B.; Norton, J. R. *J. Am. Chem. Soc.* **1982**, *104*, 6360–6368 and references therein.
(24) (a) Jeffery, J. C.; Orpen, A. G.; Robinson, W. T.; Stone, F. G. A.; Went, M. J. *J. Chem. Soc., Chem. Commun.* **1984**, 396–397. (b) Rosen, R. P.; Hoke, J. B.; Whittle, R. R.; Geoffroy, G. L.; Hutchinson, J. P.; Zubieta, J. A. *Organometallics* **1984**, *3*, 846–855. For spectrally similar μ_2-η^2-acyls whose structures do not show a contribution from the oxycarbene resonance form, see: (c) Jensen, C. M.; Knobler, C. B.; Kaesz, H. D. *J. Am. Chem. Soc.* **1984**, *106*, 5926–5933 and references therein. (d) Johnson, B. F. G.; Lewis, J.; Odiaka, T. I.; Raithby, P. R. *J. Organomet. Chem.* **1981**, *216*, C56–C60. (e) Kreiter, C. G.; Franzreb, K.-H.; Sheldrick, W. S. *J. Organomet. Chem.* **1984**, *270*, 71–79. (f) Azam, K. A.; Deeming, A. J.; Rothwell, I. P. *J. Chem. Soc., Dalton Trans.* **1981**, 91–98. It should be noted that each of these acyls are homometallic complexes.
(25) (a) Puddephatt, R. J. *Chem. Soc. Rev.* **1983**, *12*, 99–127. (b) Balch, A. In *Homogeneous* Catalysis *with Metal Phosphine Complexes*; Pignolet, L. H., Ed.; Plenum: New York, 1983.

byproduct, was minimized (<4%) via repeated washing with Et_2O. Heterobinuclear acetyl **4** was sparingly soluble in CH_2Cl_2, $CHCl_3$, and THF but virtually insoluble in hydrocarbons and aromatics. Final crystallization of **4** from hot CH_2Cl_2 or THF provided clear, light yellow plates, but these proved unsuitable for X-ray analysis. Conductance measurements carried out in CH_2Cl_2 verified the nonionic formulation.

Structure elucidation of **4** was aided by the preparation of ^{13}C isotopomers. Exposure of **4** to ^{13}CO resulted in the exchange of the terminal carbonyl to give **4**-^{13}CO; 50% enriched **3** was utilized to prepare a statistical (~1:1:1:1) mixture of **4**, **4**-$^{13}CO/^{13}COMe$, **4**-^{13}CO and **4**-$^{13}COMe$. The trans disposition of the PPh_2 units was signified by a doublet (δ 22.92 (J_{RhP} = 149 Hz)) in the $^{31}P\{^1H\}$ NMR and inequivalent methylene protons (CHH'; δ 4.06, 5.05) observed by ^1H NMR were consistent with a lone mirror plane. Primary structural evidence was obtained via examination by $^{13}C\{^1H\}$ NMR. Chemical shifts and coupling constants of the RhCO (δ 195.18 (J_{CP} = 15, J_{CRh} = 52, J_{CC} = 29 Hz)) and RhCOMe (δ 309.22 (J_{CP} = 11, J_{CRh} = 30, J_{CC} = 29 Hz)) confirmed the connectivity of the Rh core. When spectra of pure **4**-^{13}CO were compared with the overlapping resonances of the statistical, isotopomeric mixture described above, the J_{CC} was identified; corresponding $^{31}P\{^1H\}$ NMR spectra of the isotopomers allowed differentiation of J_{CRh} and J_{CP}.

IR spectra of **4** revealed a terminal CO (ν(C≡O) = 2014 cm^{-1}) and a weak absorption at 1490 cm^{-1} attributed to the acetyl ($\nu(^{13}C{=}O)$ = 1460 cm^{-1}). The latter value is low when compared to conventional η^1-COR ligands[26] but within the range of similar bridging acyls.[20,23,24] A contribution from an alternate μ_2-η^2-oxycarbene resonance form (**4'**, Figure 1) is suggested by the low-energy stretch and related low-field shift for the acetyl carbon atom (δ 309.22). Both square-planar and trigonal-bipyramidal (tbp) Rh geometries conform to the spectroscopic data while the Zr may be considered seven-coordinate, assuming Cp* occupies three sites. Molecular models of **4** indicated that the Rh and Zr, constrained by the μ_2-η^2-acetyl, should both be within the bonding range of the chloride; hence the structures shown portray a tbp configuration at Rh.

Scheme I illustrates probable pathways for the formation of acetyl **4** and the byproduct, dichloride **5**. In A, Cp*MeZr(OCH_2Ph_2P)$_2$ (**2**) cleaves the $[(OC)_2RhCl]_2$ (**3**) dimer with or without the loss of CO. A subsequent binuclear Cl for Me exchange occurs,[12,27,28] followed by the migratory insertion of a carbonyl into the new Rh–Me bond. The coordinatively unsaturated Zr center then traps the acetyl,[29] generating **4**. In B, free CO released in the course of substitution inserts into the Zr–Me bond, providing a Zr(η^2-COMe) intermediate.[30] The ensuing migration of the acetyl carbon to Rh can be rationalized by invoking an attack by the oxycarbene resonance form of this fragment[20,23,31] or by envisioning an electrophilic attack by the acyl on Rh.[32] Should bimolecular Cl for Me exchange between **3** and **2** occur (C), the Cp*ClZr(OCH_2Ph_2P)$_2$ produced would cleave **3** and form Cp*Zr(μ-OCH_2Ph_2P)$_2$(μ-Cl)$_2$RhCO (**5**), releasing CO in the process. In a typical preparation, ~0.15 equiv of CO are released according to Toepler pump measurements.

Scheme II

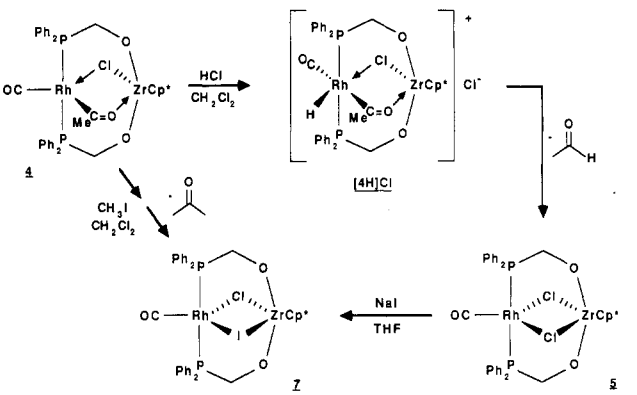

Inspection of the oxycarbene resonance form **4'** suggested that removal of the terminal CO might lead to formation of a square-planar Rh–zirconoxy carbene. Several thermal and photochemical attempts to cleanly remove or substitute for the carbonyl proved ineffective. Since plausible mechanisms of **4**'s formation involved initial loss of CO from **3**, the starting Rh-containing species was modified to contain only one CO. The addition of 2 equiv of $HOCH_2Ph_2P$ to 0.5 equiv of $[(OC)_2RhCl]_2$ (**3**) resulted in the preparation of *trans*-($HOCH_2Ph_2P$)$_2$RhCl(CO) (**6**, eq 3). Alcoholysis of

$$^1/_2\,[(OC)_2RhCl]_2 + 2HOCH_2Ph_2P \xrightarrow{-CO} \textit{trans}\text{-}(HOCH_2Ph_2P)_2RhCl(CO) \quad (3)$$

3 **6**

Cp*ZrMe_3 (**1**) with **6** did not affect the desired conversion, instead resulting in a mixture of products consistent with disproportionation pathways.

Chemistry of μ_2-η^2-Acetyl. Electrophilic reagents readily severed the μ_2-η^2-acetyl bridge of **4** as indicated in Scheme II. When subjected to 1 equiv of HCl, **4** extruded acetaldehyde in 61% yield (GC/MS, ^1H NMR) concomitant with the formation of **5**. From **4**-^{13}CO, only $H_3C^{12}CHO$ was formed (>98% by IR, ^1H NMR), ruling out possible terminal CO/acetyl CO scrambling processes and supporting direct cleavage of the bridge.[33] ^1H NMR monitoring of the reaction revealed that **5** was generated in 68% yield yet could not be cleanly isolated under the reaction conditions.[34] Thermolysis of **4** in $CDCl_3$ also resulted in moderate yields of **5** (~50% by ^1H NMR); apparently $CDCl_3$ serves as a "slow" source of D/HCl, since trace amounts of H_3CCHO could be identified in sealed NMR tube reactions.[35] The residual material obtained after isolation of **4** (eq 2) was refluxed for 1.5 h in $CHCl_3$, ultimately providing analytically pure **5** in convenient fashion. A terminal CO (ν(C≡O) = 1998 cm^{-1}), transphosphine bridges, and a single resonance for the CH_2 (δ

(26) Collman, J. P.; Hegedus, L. S.; Norton, J. R.; Finke, R. G. *Principles and Applications of Organotransition Metal Chemistry*; University Science Books: Mill Valley, CA, 1987.
(27) Garrou, P. E. *Adv. Organomet. Chem.* **1984**, *23*, 95–129.
(28) (a) Puddephatt, R. J.; Stalteri, M. A. *Organometallics* **1983**, *2*, 1400–1405. (b) Pankowski, M.; Samuel, E. *J. Organomet. Chem.* **1981**, *221*, C21–C24.
(29) Butts, S. B.; Strauss, S. H.; Holt, E. M.; Stimson, R. E.; Alcock, N. W.; Shriver, D. F. *J. Am. Chem. Soc.* **1980**, *102*, 5093–5100.
(30) Marsella, J. A.; Moloy, K. G.; Caulton, K. G. *J. Organomet. Chem.* **1980**, *201*, 389–398.
(31) (a) Marsella, J.; Huffman, J. C.; Folting, K.; Caulton, K. G. *Inorg. Chem. Acta* **1985**, *96*, 161–170. (b) Marsella, J. A.; Huffman, J. C.; Folting, K.; Caulton, K. G. *J. Am. Chem. Soc.* **1981**, *103*, 5596–5598. (c) Marsella, J. A.; Caulton, K. G. *Ibid.* **1980**, *102*, 1747–1749.
(32) Tatsumi, K.; Nakamura, A.; Hofmann, P.; Stauffert, P.; Hoffmann, R. *J. Am. Chem. Soc.* **1985**, *107*, 4440–4451.
(33) (a) Milstein, D.; Fultz, W. C.; Calabrese, J. C. *J. Am. Chem. Soc.* **1986**, *108*, 1336–1338. (b) Pruett, R. L. *Adv. Organomet. Chem.* **1979**, *17*, 1–60.
(34) Concurrent pathways leading to degradation products limited efforts to determine the molecularity of the presumed acyl–hydride reductive elimination step. See: Collman, J. P.; Belmont, J. A.; Brauman, J. I. *J. Am. Chem. Soc.* **1983**, *105*, 7288–7294.
(35) Presumably the appearance of H_3CCOH results from the rapid exchange of DCl with protons on the surface of the NMR tube.

5.15) groups corroborate the symmetric structure indicated.

At intermediate stages of the HCl cleavage, the ^1H NMR spectrum was dominated (37% maximum) by the presence of complex tentatively formulated as [Cp*Zr(μ-OCH_2Ph_2P)$_2$(μ_2-η^2-O=C(CH_3))(μ-Cl)Rh(CO)H]Cl ([**4H**]**Cl**). In the ^1H NMR spectrum, a Rh–H at δ −15.21 (J_{RhH} = 28, J_{PH} = 9 Hz), new multiplets corresponding to CHH′ groups (δ 5.10, 5.60), and a new acetyl at δ 1.05 were diagnostic for the transient acetyl–hydride. The $^{31}P\{^1H\}$ NMR spectrum again manifested trans-phosphine bridges (δ 14.26 (J_{RhP} = 98 Hz)) while the IR spectrum revealed a terminal CO stretch at 2097 cm^{-1} ($\nu(^{13}CO)$ = 2050 cm^{-1}) and a new acetyl C=O stretch at 1542 cm^{-1} ($\nu(^{13}C{=}O)$ = 1508 cm^{-1}). These shifts to higher energy relative to those in **4** are consistent with the formal oxidation of the Rh(I) center to Rh(III),[36] rendering less π-back-bonding to the CO and acetyl.

Since the acetyl–hydride [**4H**]**Cl** presumably served as the precursor to **5** via the reductive elimination of acetaldehyde,[33,34] RX electrophiles were expected to yield ketones.[37] In accord with this prediction, **4** was treated with methyl iodide (~1.8 equiv) as shown in Scheme II. Acetone was generated in 93% yield (GC, ^1H NMR) along with Cp*Zr(μ-OCH_2Ph_2P)$_2$(μ-Cl)(μ-I)RhCO (**7**), formed in 85% yield (^1H NMR). On a larger scale, **7** could be isolated in 72% yield or prepared from **5** and excess NaI in THF, although this method appeared to produce some of the corresponding diiodide. Exposure of **4**-^{13}CO to CH_3I eliminated $Me_2{}^{12}CO$ (>98% by ^1H NMR, IR), again supporting direct cleavage of the bridge. In contrast to symmetric **5**, the CHH′ units of the iodo–chloride **7** were observed as two multiplets (δ 5.33, 5.45) indicative of a lone mirror plane containing Cl, I, and both metals. The overall rates of MeCHO and Me_2CO formation were comparable ($t_{1/2} \approx$ 2 days) under similar conditions (1 equiv of electrophile, 25 °C, CH_2Cl_2) implicating slow electrophilic attack by MeI relative to HCl, since no intermediates were observed in the former reaction.

Complexes Containing Rh–Zr Bonds. Treatment of Cp*ZrMe(OCH_2Ph_2P)$_2$ (**2**) with (Ph_3P)$_3$RhMe (**8a**)[38] in toluene afforded light yellow Cp*Zr(μ-OCH_2Ph_2P)$_2$RhMe$_2$ (**9**), a complex containing a Rh–Zr bond (eq 4). Cp*Zr(μ-OCH_2Ph_2P)$_3$RhMe (**11**), generated

$$\underset{\mathbf{2}}{\text{Cp*ZrMe}(OCH_2Ph_2P)_2} + \underset{\mathbf{8a}}{(Ph_3P)_3RhMe} \xrightarrow[-3Ph_3P]{\text{toluene, 25 °C}} \underset{\mathbf{9}\ (\sim 75\%)}{\text{Cp*Zr}(\mu\text{-}OCH_2Ph_2P)_2RhMe_2} \quad (4)$$

via an unknown disproportionation pathway, was produced as a sporadic impurity in variable amounts. Tribridged **11** was independently synthesized in 81% yield by an in situ alcoholysis of Cp*ZrMe$_3$ (**1**) with 3 equiv of $HOCH_2Ph_2P$ to provide Cp*Zr(OCH_2Ph_2P)$_3$ (**10**, eq 5), followed by the addition of (Ph_3P)$_3$RhMe (**8a**, eq 6).

$$\underset{\mathbf{1}}{\text{Cp*ZrMe}_3} + 3HOCH_2Ph_2P \xrightarrow{-3CH_4} \underset{\mathbf{10}}{\text{Cp*Zr}(OCH_2Ph_2P)_3} \quad (5)$$

$$\underset{\mathbf{10}}{\text{Cp*Zr}(OCH_2Ph_2P)_3} + \underset{\mathbf{8a}}{(Ph_3P)_3RhMe} \xrightarrow{-3Ph_3P} \underset{\mathbf{11}}{\text{Cp*Zr}(\mu\text{-}OCH_2Ph_2P)_3RhMe} \quad (6)$$

During isolation of the heterobimetallic complexes derived from (Ph_3P)$_3$RhR, complete removal of byproduct Ph_3P proved difficult. Although separation of Ph_3P from **9** was accomplished via recrystallization, as determined by NMR spectroscopy, satisfactory combustion analyses could not be obtained. Confirmation of the structure resulted from X-ray diffraction studies (vide infra). Difficulties in obtaining satisfactory analyses have been previously encountered with heterobimetallics containing the μ-OCH_2Ph_2P ligand.[10-12] In all cases herein, estimates of purity based on ^{31}P, ^{13}C, and ^1H NMR studies are provided in the Experimental Section.

Some curious spectral features initially suggested that **9** contained an unanticipated Zr–Rh bond. The methyl groups exhibited a multiplet in the ^1H NMR at δ 0.63 which retained its shape when **9** was synthesized from Cp*Zr(CD_3)(OCH_2Ph_2P)$_2$ (**2**-d_3). The $^{13}C\{^1H\}$ NMR spectrum manifested an AXX′M pattern for the RhMe at δ 4.23 with 76-, 23-, and 10-Hz couplings tentatively assigned to the trans phosphine, Rh, and the cis phosphine, respectively. While the $^{31}P\{^1H\}$ NMR spectrum indicated one type of bridge, inequivalent methylene protons were evident and some phenyl multiplets were observed upfield (δ 6.56, 6.71) of their usual positions. Similar shifts noted for various *cis*-(dppe)$_2$MX$_2$ complexes have been attributed to close ortho-H/X contacts,[39] foreshadowing a constrained geometry of the bridges. Cryoscopic molecule weight measurements (found, 793; calcd, 790) supported the binuclear formulation. Reactivity studies were also consistent with the structure presented; **9** did not react when exposed to CO_2[40] and N_2O[41] for prolonged periods at 25 °C, a pattern inconsistent with the potential presence of a ZrMe bond. At higher temperatures or when subjected to harsher reagents such as HCl, **9** decomposed to complex mixtures of products. The unreactive nature of the Rh–Zr bond was puzzling in view of its expected polarity, Rh(δ−)–Zr(δ+), but consistent with a dramatic steric shielding by the coordination spheres of both metals (vide infra).

In order to extend this study of early/late metal–metal bonded complexes, we treated (Ph_3P)$_3$RhH (**8b**)[42] with Cp*ZrMe(OCH_2Ph_2P)$_2$ (**2**), causing the immediate evolution of methane (0.96 equiv). Cp*Zr(μ-OCH_2Ph_2P)$_2$RhPPh_3 (**12**) could be isolated from a dark burgundy solution as a rose-colored powder (eq 7); efforts

$$\underset{\mathbf{2}}{\text{Cp*ZrMe}(OCH_2Ph_2P)_2} + \underset{\mathbf{8b}}{(Ph_3P)_3RhH} \xrightarrow{Et_2O} CH_4 + (2-x)PPh_3 + \underset{\mathbf{12}}{\text{Cp*Zr}(\mu\text{-}OCH_2Ph_2P)_2RhPPh_3\cdot xPPh_3} \quad (7)$$

to separate residual Ph_3P from **12** were ineffective, hence "purified" material contained at least 0.4 equiv of Ph_3P. Inequivalent methylene protons and a $^{31}P\{^1H\}$ NMR resonance at δ 13.25 (dd, J_{RhP} = 213, J_{PP} = 66 Hz) characterized the bridging units while a doublet of triplets at δ 41.74 (J_{RhP} = 176, J_{PP} = 66 Hz) was attributed to the Ph_3P ligand. The J_{PP} of 66 Hz is atypical of cis (20–40 Hz) and trans (>300 Hz) couplings of square-planar P_2Rh units[43]

(36) Tiethof, J.; Petersen, J. L.; Meek, D. W. *Inorg. Chem.* **1976**, *15*, 1365–1370.
(37) Suggs, W. J.; Wovkulich, M. J.; Cox, S. D. *Organometallics* **1985**, *4*, 1101–1107 and references therein.
(38) Keim, W. *J. Organomet. Chem.* **1968**, *14*, 179–184.
(39) (a) Lilga, M. Z.; Ibers, J. A. *Inorg. Chem.* **1984**, *23*, 3538–3543. (b) Ginsberg, A. P.; Lindsell, W. E. *Ibid.* **1973**, *12*, 1983–1985. (c) Lilga, M. A.; Ibers, J. A. *Organometallics* **1985**, *4*, 590–598.
(40) The analogous treatment of Cp*ZrMe(μ-OCH_2Ph_2P)$_2$PtMe$_2$ (ref 12) with CO_2 provides Cp*Zr(O_2CMe)(μ-OCH_2Ph_2P)$_2$PtMe$_2$: Ferguson, G. S.; Ph.D. thesis, Cornell University, 1987.
(41) Vaughan, G. A.; Rupert, P. B.; Hillhouse, G. L. *J. Am. Chem. Soc.* **1987**, *109*, 5538–5539.
(42) Keim, W. *J. Organomet. Chem.* **1967**, *8*, P25–P26.
(43) Pregosin, P. S.; Kunz, R. W. *NMR 16: Basic Principles and Progress*; Diehl, P., Fluck, E., Kosfeld, R., Eds.; Springer-Verlag: Berlin, 1979; pp 119–123.

Scheme III

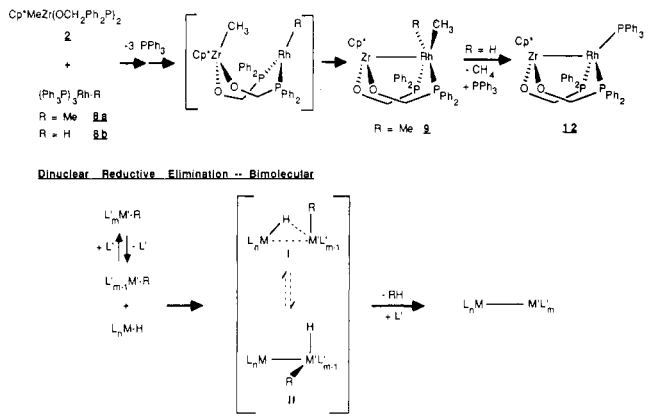

and is interpreted as indicating a pseudotetrahedral geometry about the Rh.

The formation of both **9** and **12** is reminiscent of the final, product-forming step of dinuclear reductive elimination reactions that do not involve radical chains.[44-48] As Scheme III indicates, the generation of the Zr–Rh bonds can be thought of as occurring via initial displacement of phosphine from **8a,b** by $Cp^*ZrMe(OCH_2Ph_2P)_2$ (**2**) to give a binuclear complex, followed by the oxidative addition of the Zr–Me bond across the Rh. Whereas the Rh–dimethyl fragment of **9** is stable, the RhH(Me) intermediate is susceptible to reductive elimination of CH_4, ultimately providing **12**. In the aforementioned dinuclear studies, unimolecular steps prior to bimetallic interaction have proven to be rate-determining, thereby hindering direct investigation of the reductive elimination step. The generic example in Scheme III shows two precursors to the dinuclear reductive elimination of HR. Note that the illustrated $L_nM(\mu\text{-}H)M'RL'_{m-1}$ intermediate/transition state species[44,47,49,50] (I) is a minor perturbation of the more formal $L_nM\text{–}M'H(R)L'_{m-1}$ (II) description. The pathway to and stability of $Cp^*Zr(\mu\text{-}OCH_2Ph_2P)_2RhMe_2$ (**9**) suggests that generation of the latter precedes dinuclear reductive elimination, at least in the case of **12**. By inference, similar intramolecular dinuclear 1,2-eliminations,[51] considered to be thermally forbidden,[52,53] may be disfavored with respect to H or R migration and subsequent 1,1-elimination.

Excess H_2 quickly discharged the dark burgundy color of $Cp^*Zr(\mu\text{-}OCH_2Ph_2P)_2RhPPh_3$ (**12**) in benzene, producing a gold-orange solution of $Cp^*Zr(\mu\text{-}OCH_2Ph_2P)_2RhH_2(PPh_3)$ (**13**, Scheme IV) in near quantitative yield by ^1H NMR. Since the problems with PPh_3 impurity in **12** persisted, **13** was prepared in alternate fashion through the hydrogenation of $Cp^*Zr(\mu\text{-}OCH_2Ph_2P)_2RhMe_2$ (**9**) with 1.0 equiv of PPh_3 present;[48] 1.9 equiv of CH_4 are produced and **12** was observed as an intermediate. The ^1H NMR of **13** displayed a broad RhH_2 resonance at δ −7.17 (toluene-d_8, dd, $J_{t\text{-}PH}$ = 72 (corroborated via ^{31}P NMR), J_{RhH} = 28 Hz, $\nu_{1/2}$(av) = 24 Hz)[43,54] but otherwise spectrally resembled **9** and **12**, implicating a similarly bridged structure.[55] At 21 °C, a single $^{31}P\{^1H\}$ resonance for the bridges was observed at δ 31.56 (C_6D_6, d, J_{RhP} = 130 Hz) accompanied by a broad $[PPh_3]$-dependent signal, indicative of reversible PPh_3 loss. Further complications arose at lower temperatures. In the ^1H NMR spectrum, the broad doublet of triplets observed at 0 °C partially resolved to a symmetric doublet ($J_{t\text{-}PH}$ = 102 Hz) of "triplet" ($J_{RhH} \simeq J_{HP}$ = 28 Hz) of doublets ($J_{c\text{-}PH}$ = 12 Hz) at −19 and −50 °C. These tentative assignments are consistent with loss of coupling due to PPh_3 at higher temperatures. The corresponding change in the $^{31}P\{^1H\}$ spectrum was not as straightforward. At 0 °C an apparent doublet of doublets at δ 32.87 (br, J_{RhP} = 130, "$J_{PP'}$" = 27 Hz) revealed that phosphorus atoms of the bridges were inequivalent and coupling due to the bound PPh_3 (δ 30.32 (br d, J_{RhP} = 82 Hz)) was not resolved. At −19 °C and below, further splitting resulted in the appearance of an ABXM pattern, where A and B ($J_{ARh} \approx J_{BRh}$ = 128 Hz at −49 °C) are the inequivalent phosphorus atoms of the bridges and X (J_{XRh} = 89 Hz at −49 °C) is the PPh_3.

There is an apparent contradiction in the two sets of data since the hydrides are observed as equivalent in contrast to the phosphine bridges. Two explanations are

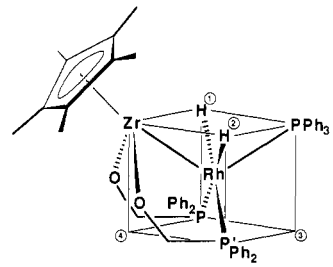

Figure 2.

Scheme IV

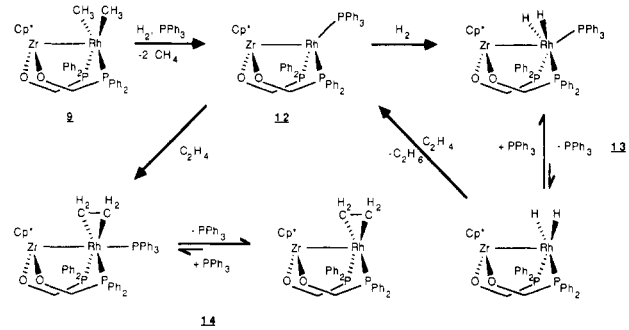

(44) (a) Martin, B. D.; Warner, K. E.; Norton, J. R. *J. Am. Chem. Soc.* **1986**, *108*, 33–39. (b) Warner, K. E.; Norton, J. R. *Organometallics* **1985**, *4*, 2150–2160.

(45) (a) Carter, W. J.; Okrasinski, S. J.; Norton, J. R. *Organometallics* **1985**, *4*, 1376–1386. (b) Norton, J. R. *Acc. Chem. Res.* **1979**, *12*, 139–145.

(46) (a) Nappa, M. J.; Santi, R.; Halpern, J. *Organometallics* **1985**, *4*, 34–41. (b) Halpern, J. *Acc. Chem. Res.* **1982**, *15*, 332–338. (c) Halpern, J. *Inorg. Chem. Acta* **1982**, *62*, 31.

(47) Jones, W. D.; Huggins, J. M.; Bergman, R. G. *J. Am. Chem. Soc.* **1981**, *103*, 4415–4423.

(48) Janowicz, A. H.; Bergman, R. G. *J. Am. Chem. Soc.* **1981**, *103*, 2488–2489.

(49) For relevant bridging hydrides, see: (a) Venanzi, L. M. *Coord. Chem. Rev.* **1982**, *43*, 251–274. (b) Hill, R. H.; Puddephatt, R. J. *J. Am. Chem. Soc.* **1983**, *105*, 5797–5804 and references therein.

(50) Casey, C. P.; Rutter, E. W., Jr.; Haller, K. J. *J. Am. Chem. Soc.* **1987**, *109*, 6886–6887.

(51) (a) Chetcuti, M. J.; Chisholm, M. H.; Folting, K.; Haitko, D. A.; Huffman, J. C. *J. Am. Chem. Soc.* **1982**, *104*, 2138–2146. (b) Chisholm, M. H.; Huffman, J. C.; Tatz, R. J. *Ibid.* **1983**, *105*, 2075–2077.

(52) Hembre, R. T.; Scott, C. P.; Norton, J. R. *J. Am. Chem. Soc.* **1987**, *109*, 3468–3470.

(53) Trinquier, G.; Hoffmann, R. *Organometallics* **1984**, *3*, 370–380.

(54) For a RhH/Zr bimetallic with related spectral features, see: Choukroun, R.; Iraqi, A.; Gervais, D.; Daran, J.-C.; Jeannin, Y. *Organometallics* **1987**, *6*, 1197–1201.

(55) For examples of early/late M–M′ complexes containing hydrides, see: (a) Bruno, J. W.; Huffman, J. C.; Green, M. A.; Caulton, K. G. *J. Am. Chem. Soc.* **1984**, *106*, 8310–8312. (b) Bars, O.; Braunstein, P.; Geoffroy, G. L.; Metz, B. *Organometallics* **1986**, *5*, 2021–2030 and references therein.

proffered: (1) the low-temperature proton NMR signals are broad, and hence the hydrides are different yet near in chemical shift and therefore unresolved; and (2) the hydrides are made equivalent by a process separate from that which averages the bridges. The latter postulate is plausible in view of Muetterties analysis of the hydride movements in P_4MH_2 (M = Fe, Ru) complexes.[56,57] The $^{31}P\{^1H\}$ NMR data point to the association of PPh_3 as the process by which the bridge phosphorus atoms become inequivalent. Presumably, the added steric influence of the PPh_3, in combination with the hydrides, generates a particular low-energy conformation of the bridges; a juxtaposition of the bridges' phenyl groups renders the P atoms inequivalent. While not easily visualized, precedent for a conformational preference is indicated by the structure of **9** (vide infra). A low-temperature structure for **13** in which a cube has been overlaid is illustrated in Figure 2. As in the P_4MH_2 cases, the bulky substituents, in this case the phosphines and Cp*Zr moiety, occupy pseudotetrahedral positions. The hydride ligands are thus free to migrate (tetrahedral hop) to all other corners (1–4) of the cube in a process which results in their interconversion, despite having a surrounding molecular framework which manifests four different sites.

Infrared spectra of **13** are consistent with the structure depicted in Figure 2. A broad IR band at 1747 cm^{-1} (benzene solution) assigned to the Rh–H stretch (ν(RhD) = 1259 cm^{-1}),[55] while failing to concretely distinguish between bridged and terminal hydride geometries, is nonetheless supportive of the structure implicated. Elemental analysis of **13** again proved problematic, although satisfactory purity was obtained, as determined via ^1H, $^{13}C\{^1H\}$, and $^{31}P\{^1H\}$ NMR spectroscopy (see Experimental Section).

Disappointing results were obtained when dihydride **13** was exposed to selected small molecules. While complex mixtures were obtained from CO, CO_2, HCl, and MeI treatments, ethylene was slowly hydrogenated by **13** to give ethane and $Cp^*\overline{Zr(\mu\text{-}OCH_2Ph_2P)_2}RhPPh_3$ (**12**, Scheme IV). In the presence of excess ethylene, **13** was converted to an ethylene adduct, $Cp^*\overline{Zr(\mu\text{-}OCH_2Ph_2P)_2}Rh(\eta\text{-}C_2H_4)$ (**14**), and PPh_3. Adduct **14** possessed the typical pattern for μ-OCH_2Ph_2P bridges that span a Zr–Rh bond and two distinct types of coupled olefin protons at δ 2.25 and 3.04 (J = 11 Hz), with the former exhibiting some additional coupling (1.5 Hz). The $^{13}C\{^1H\}$ NMR spectrum exhibited a doublet (J_{RhC} = 10 Hz)[58,59] of virtual triplets (J_{PC} = 6 Hz) for the equivalent ethylene carbon atoms at δ 37.83, and the phosphorus atoms of the bridges were observed as a doublet by $^{31}P\{^1H\}$ NMR (δ 15.35 (J_{RhP} = 177 Hz). The data point to a structure for **14** similar to the dimethyl **9** with the ethylene carbons positioned akin to the methyls of the latter. Removal of byproduct PPh_3 again proved difficult, and unless excess C_2H_4 was present, **14** slowly reverted to **12** via substitution of the ethylene.[58] Furthermore, the PPh_3 resonance was slightly shifted and broadened from its free value ($^{31}P\{^1H\}$), and the resonance for excess ethylene, when present, was broadened in the $^{13}C\{^1H\}$ spectrum, indicating that these ligands reversibly bind to the apical position of the square pyramid, albeit very weakly. Although analytical difficulties due to ubiquitous PPh_3 were encountered, note that Rh–Zr bonded compounds **12–14** can be generated via structurally characterized **9** under conditions of known stoichiometry (eq 7, Scheme IV), thereby providing a chemical check of their constituents.

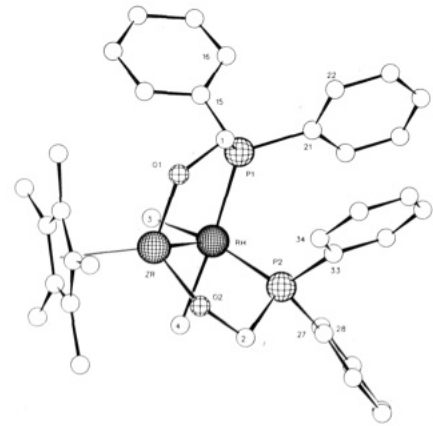

Figure 3. Molecular structure of $Cp^*\overline{Zr(\mu\text{-}OCH_2Ph_2P)_2}RhMe_2$ (**9**). Numbers refer to carbon atoms.

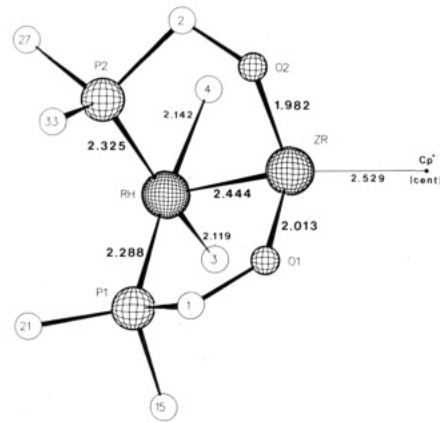

Figure 4. Inner coordination sphere of $Cp^*\overline{Zr(\mu\text{-}OCH_2Ph_2P)_2}RhMe_2$ (**9**). Distances are in angstroms (Å), and numbers refer to carbon atoms.

Table I. Selected Interatomic Distances (Å) and Angles (deg) for $Cp^*\overline{Zr(\mu\text{-}OCH_2Ph_2P)_2}RhMe_2$ (9)

Rh–Zr	2.444 (1)	P1–C1	1.857 (16)
Rh–C3	2.119 (13)	P2–C2	1.882 (11)
Rh–C4	2.142 (16)	O1–C1	1.424 (12)
Rh–P1	2.288 (4)	O2–C2	1.410 (14)
Rh–P2	2.325 (4)	P1–C15(Ph)	1.828 (13)
Zr–O1	1.982 (10)	P1–C21(Ph)	1.816 (10)
Zr–O2	2.013 (9)	P2–C27(Ph)	1.814 (15)
Zr–Cp*(cent)	2.259	P2–C33(Ph)	1.839 (15)
Cp*–Zr–Rh	138.3	Zr–Rh–P1	92.1 (1)
Cp*–Zr–O1	106.9 (4)	Zr–Rh–P2	86.8 (1)
Cp*–Zr–O2	110.6 (4)	Zr–Rh–C3	101.0 (2)
O1–Zr–O2	106.8 (2)	Zr–Rh–C4	83.1 (2)
Rh–Zr–O1	93.7 (1)	Rh–P1–C1	107.8 (2)
Rh–Zr–O2	97.3 (1)	Rh–P2–C2	108.3 (2)
P1–Rh–P2	98.1 (1)	P1–C1–O1	109.1 (4)
C3–Rh–C4	83.4 (4)	P2–C2–O2	106.5 (4)
P1–Rh–C3	94.9 (3)	Zr–O1–C1	129.8 (3)
P2–Rh–C4	84.3 (3)	Zr–O2–C2	126.5 (3)
P1–Rh–C4	174.5 (2)		
P2–Rh–C3	164.5 (2)		

X-ray Structural Investigation of $Cp^*\overline{Zr(\mu\text{-}OCH_2Ph_2P)_2}RhMe_2$ (9). Crystals of $Cp^*\overline{Zr(\mu\text{-}OCH_2Ph_2P)_2}RhMe_2$ (**9**), suitable for X-ray diffraction

(56) (a) Meakin, P.; Muetterties, E. L.; Jesson, J. P. *J. Am. Chem. Soc.* **1973**, *95*, 75–88. (b) Meakin, P.; Muetterties, E. L.; Tebbe, F. N.; Jesson, J. P. *Ibid.* **1971**, *93*, 4701–4709.

(57) Muetterties, E. L. *Acc. Chem. Res.* **1970**, *3*, 266–273.

(58) Tolman, C. A.; Meakin, P. Z.; Lindner, D. L.; Jesson, J. P. *J. Am. Chem. Soc.* **1974**, *96*, 2762–2774.

(59) Bodnar, G. M.; Storhoff, B. N.; Doddrell, D.; Todd, L. J. *J. Chem. Soc., Chem. Commun.* **1970**, 1530–1531.

studies, were grown via slow vapor diffusion of hexane into toluene. Structure refinement (triclinic, $P\bar{1}$) using heavy-atom techniques proceeded routinely, resulting in a residual (R) of 0.063 (R_w = 0.051). Figure 3 displays the molecular structure of **9** as viewed from the Zr–Rh side of the complex, and Figure 4 exhibits a skeletal view, with the phenyl and Cp* methyl carbons removed for clarity. Pertinent interatomic distances and bond angles are listed in Table I.

The local geometry about rhodium is essentially square-pyramidal, with the phosphines and methyl groups comprising the base and the Zr atom positioned in the apical site. The Rh–P bond lengths (2.288 (4), 2.325 (4) Å) are similar to those in other phenylphosphine-containing Rh compounds,[60] and normal Rh–Me distances (2.119 (13), 2.142 (16) Å) are manifested.[61,62] No significant displacement of Rh from the basal plane is indicated by the Zr–Rh–L angles (91 (8)° average; L = Me, PPh_2–), but the plane is slightly twisted such that C4 is displaced toward Zr and C3 away. It appears that phenyl groups of adjacent cis phosphines align in a face-to-face arrangement in order to alleviate steric strain, imparting a twist to the Ph_2P fragments that is transmitted to the Me groups in the basal plane. A conformational bias of this type may be responsible for the low-temperature inequivalence of the bridged phosphines of dihydride **13**. Angles within the base average 90 (7)°, but the deviations are significant and originate from the size of the ligands (e.g. ∠P1–Rh–P2 = 98.1 (1)°).

The zirconium coordination sphere is most easily described as a distorted tetrahedron, with the large Cp* and P_2RhMe_2 substituents separated by 138.3 (1)°. The O–Zr–O angle of 106.8 (2)° and Cp*(centroid)–Zr–O angles (106.9 (4), 110.6 (4)°) are near the tetrahedral ideal, but the Rh–Zr–O angles (93.7 (1), 97.3 (1)°) are clearly compressed. Despite the close Zr–Rh interaction, the P–C–O angles (106.5 (4), 109.1 (4)°) indicate that the bridges are relatively strain-free. Typical Cp*–Zr (2.57 (4) Å average)[63] and somewhat long Zr–O distances (1.982 (10), 2.013 (9) Å)[64,65] are observed. In comparison to related complexes,[10,65] the C–O–Zr angles (129.8 (3), 126.5 (3)°) are less obtuse, implying less oxygen π-donation to the Lewis acidic zirconium center in accord with the longer Zr–O bond distances.

The most striking feature of the structure is the 2.444 (1) Å Rh–Zr bond, one of the shortest heterobimetallic distances discovered.[5,66,67] Since the sum of the covalent radii of Zr and Rh is 2.70 Å, multiple bonding must be considered. The combination of the electron-rich Rh and Lewis acidic, electron-poor Zr encourages Rh→Zr $d\pi$–$d\pi$ bonding in a manner similar to transition-metal backbonding with main-group π-acids.[68] One may view this bimetallic as a donor/acceptor complex by considering the square-planar $[P_2RhMe_2]^-$ moiety σ- and π-donating to a cationic $[Cp^*Zr(OR)_2]^+$ fragment. Calculations probing the nature of this interaction are presented below.

Most square-planar and square-pyramidal bis(phosphine)rhodium complexes exhibit trans geometries,[69] yet the configuration of $Cp^*Zr(\mu\text{-}OCH_2Ph_2P)_2RhMe_2$ (**9**) is cis. Since the geometry about the Zr is sterically and electronically constrained to be pseudotetrahedral, the orientation of the Zr–alkoxide linkages is transposed through the bridges to the Rh center, engendering the cis-phosphine structure. The *cis*-RhP_2Me_2 conformation also minimizes Cp*/phenyl steric interactions, at the cost of increased interbridge phenyl/phenyl steric influences, indicated by the aforementioned opening of the P1–Rh–P2 angle and the basal plane twist. Clearly, the flexibility of the alkoxymethyldiphenylphosphine bridge accommodates a short, strong intermetallic link; both Figures 3 and 4 indicate that the RhP_2Me_2 square plane is slightly canted toward the Zr. The structure also provides an explanation for the compounds surprisingly unreactive character. The Rh–Zr bond, initially expected to be a reactive functionality, is buried within a shield of Cp* and Ph groups, thereby guarded from attack. Furthermore, the strength of the short Rh–Zr bond must lessen its susceptibility to electrophilic attack and oxidative additions.

Extended Hückel Calculations on M–M′ Bonds. In order to more fully understand the components of bonding in $Cp^*Zr(\mu\text{-}OCH_2Ph_2P)_2RhMe_2$ (**9**), we performed an extended Hückel (EH) calculation on a model complex, $Cp(HO)_2Zr\text{-}Rh(PH_3)_2Me_2$ (**9′**), using appropriately idealized bond distances and angles from the crystallographic study. For comparison, pertinent heterobimetallic complexes were modeled in a likewise manner: (1) $Cp_2(O\text{-}t\text{-}Bu)Zr\text{-}RuCp(CO)_2$[70] was examined as $Cp_2(HO)Zr\text{-}RuCp(CO)_2$ (I); (2) $Cp^*Rh(\mu\text{-}PMe_2)_2Mo(CO)_4$,[71] a species whose Rh–Mo bond description is dependent on the choice of formal oxidation states, was treated as $CpRh(\mu\text{-}PH_2)_2Mo(CO)_4$ (II); (3) the MeI oxidative addition product of the latter, *mer*-$Cp^*MeRh(\mu\text{-}PMe_2)_2Mo(CO)_3I$,[62] was simplified to *mer*-$CpMeRh(\mu\text{-}PH_2)_2Mo(CO)_3I$ (III); and (4) calculations modeling $Cp(CO)Mo(\mu\text{-}CO)_2Rh(PPh_3)_2$[67] were conducted on $Cp(CO)Mo(\mu\text{-}CO)_2Rh(PH_3)_2$ (IV). These specific complexes were chosen because of the commonality of the early/late metal with **9**. In each case the M–M′ overlap population (op), presumably the most direct indicator of the type of metal–metal interaction,[72] was separated into contributions from various critical orbitals. The details of the comparative models have been

(60) For examples, see: (a) Anderson, M. P.; Pignolet, L. H. *Inorg. Chem.* **1981**, *20*, 4101–4107. (b) Faranone, F.; Bruno, G.; Tresoldi, G.; Faranone, G.; Bombieri, G. *J. Chem. Soc., Dalton Trans.* **1981**, 1651–1656. (c) Mingos, D. M. P.; Minshall, P. C.; Hursthouse, M. B.; Malik, K. M. A.; Willoughby, S. D. *J. Organomet. Chem.* **1980**, *181*, 169–182. (d) Hitchcock, P. B.; McPartlin, M.; Mason, R. *J. Chem. Soc., Chem. Commun.* **1969**, 1367–1368.

(61) Park, J. W.; Mackenzie, P. B.; Schaefer, W. P.; Grubbs, R. H. *J. Am. Chem. Soc.* **1986**, *108*, 6402–6404.

(62) Finke, R. G.; Gaughan, G.; Pierpont, C.; Noordik, J. H. *Organometallics* **1983**, *2*, 1481–1483.

(63) Wolczanski, P. T.; Threlkel, R. S.; Santarsiero, B. D. *Acta Crystallogr. Sect. C: Cryst. Struct. Commun.* **1983**, *C39*, 1330–1333.

(64) Lubben, T. V.; Wolczanski, P. T.; Van Duyne, G. D. *Organometallics* **1984**, *3*, 977–983 and references therein.

(65) Feher, F. J. *J. Am. Chem. Soc.* **1986**, *108*, 3850–3852.

(66) For other short M–M′ bonds, see: (a) King, M.; Holt, E. M.; Radnia, P.; McKennis, J. S. *Organometallics* **1982**, *1*, 1718–1720. (b) Green, M.; Hankey, D. R.; Howard, J. A. K.; Louca, P.; Stone, F. G. A. *J. Chem. Soc., Chem. Commun.* **1983**, 757–758. (c) Farr, J. P.; Olmstead, M. M.; Balch, A. L. *Inorg. Chem.* **1983**, *22*, 1229–1235. (d) Azar, M. C.; Chetcuti, M. J.; Eigenbrot, C.; Green, K. A. *J. Am. Chem. Soc.* **1985**, *107*, 7209–7210 and references therein.

(67) Carlton, L.; Lindsell, W. E.; McCullough, K. J.; Preston, P. N. *J. Chem. Soc., Chem. Commun.* **1982**, 1001–1003.

(68) Muir, K. W.; Ibers, J. A. *Inorg. Chem.* **1970**, *9*, 440–447.

(69) Hughes, R. P. *Comprehensive Organometallic Chemistry*; Wilkinson, G., Stone, F. G. A., Abel, E. W., Eds.; Pergamon: New York, 1982; Vol. 5, pp 277–540.

(70) Casey, C. P.; Jordan, R. F.; Rheingold, A. L. *J. Am. Chem. Soc.* **1983**, *105*, 665–667.

(71) Finke, R. G.; Gaughan, G.; Pierpont, C.; Cass, M. E. *J. Am. Chem. Soc.* **1981**, *103*, 1394–1399.

(72) Consider the overlap populations (op) to be scaled to the bond strength of a particular set of elements. It should be emphasized that the relative M–M′ bond strengths of the examples used may not correspond to their relative op values, although the commonality of metals in **9′** and I–IV suggests that some correlation is likely.

Compound	$Cp^*Zr(\mu\text{-}OCH_2Ph_2P)_2RhMe_2$ (9)	$Cp_2(^tBuO)Zr\text{-}RuCp(CO)_2$	$Cp^*Rh(\mu\text{-}PMe_2)_2Mo(CO)_4$	$mer\text{-}Cp^*MeRh(\mu\text{-}PMe_2)_2Mo(CO)_3I$	$Cp(CO)Mo(\mu\text{-}CO)_2Rh(PPh_3)_2$
Model	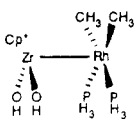	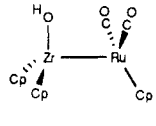	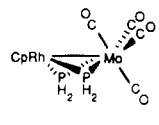	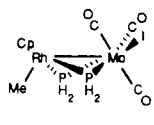	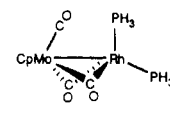
	9′	I	II	III	IV

Total Overlap Population (o.p.)	0.649	0.336	0.010	0.063	0.185
Sigma o.p.	0.306	0.275	0.039	0.087	0.143
Pi o.p.	0.343	0.061	-0.029	-0.027	0.042
d(M-M')	2.444 Å	2.910 Å	2.921 Å	2.957 Å	2.588 Å
Sum of M and M' Covalent Radii	2.70 Å	2.70 Å	2.55 Å	2.55 Å	2.55 Å

Figure 5.

purposely omitted in order to focus on these important factors.

Figure 5 lists the overlap due to σ-type orbitals, π-type combinations, and the total overlap population along with the M–M′ distance and sum of the covalent radii. A perusal of the data reveals that there is no obvious correlation between M–M′ distance and overlap population. The observation that the intermetallic distance is not particularly responsive to electronic effects can be traced to the predominantly σ-character of these metal–metal interactions. At the distances (~2.5–3.0 Å) utilized in this study, the overlap between typical σ-type orbitals, such as d_{z^2} or p_z combinations, is relatively unperturbed by bond distance changes. The overlap between π-orbitals is more responsive to distance, since it depends significantly on the directionality of the orbitals involved.[73] For example, as the Zr–Rh distance in $Cp(HO)_2Zr\text{–}Rh(PH_3)_2Me_2$ (9′) is changed from 2.444 to 2.910 Å, the total overlap decreases from 0.649 to 0.438 (–33%), due primarily to the drop in π-op from 0.343 to 0.160 (–53%). In fact, at 2.910 Å, the σ-op is 0.275 (–10%), the same as calculated for $Cp_2(HO)Zr\text{–}RuCp(CO)_2$ (I) in accord with the similar covalent radii attributed to the late metals. Correspondingly, if the Ru–Zr distance in I is compressed to 2.444 Å, the σ-op changes from 0.275 to 0.308 (+12%) while the π-op more than doubles from 0.061 to 0.162.

Both $CpRh(\mu\text{-}PH_2)_2Mo(CO)_4$ (II) and $CpMeRh(\mu\text{-}PPh_2)_2MoI(CO)_3$ (III) have a negligible Rh–Mo overlap population despite intermetallic distances indicative of a discrete bond. Finke[62] and others[74] have addressed the significance of the bridging phosphido groups on metal–metal interactions, and these calculations relate similar findings. While the dative descriptions pertaining to II (Rh(I):⩾Mo(II)) and III (Rh(III):⩾Mo(II)) provided by Finke are the most reasonable ways in which these complexes may be formally addressed, the intermetallic distances are likely a consequence of restrictions imposed by the bridging phosphides. In fact, the calculations indicate that a critical Rh σ-orbital in II interacts preferentially more with a carbonyl ligand on Mo (op = 0.05) rather than the Mo itself.

The remaining examples are of greater relevance in comparison to $Cp(HO)_2Zr\text{–}Rh(PH_3)_2Me_2$ (9′), since each contains a M–M′ bond that can justifiably be considered nondative. The Ru–Zr interaction in $Cp_2(HO)Zr\text{–}RuCp(CO)_2$ (I) is apparently dominated by steric constraints, since the bond distance appears disproportionately long (2.91 Å) with respect to calculated overlaps and the sum of Ru and Zr covalent radii (2.70 Å). The sterically favorable orientation of the Ru fragment such that its Cp is "between" those of the Cp_2Zr moiety and away from the latter's OH (O-*t*-Bu) forces the carbonyl ligands into the bent sandwich wedge while limiting overlap between appropriate Ru and Zr π-orbitals. The $CpRu(CO)_2$ also faces competition from the OH (O-*t*-Bu) group in π-donating to the formally 16e Zr center,[30,75] which has only one π-type orbital. Thus competition from the alkoxide and steric factors serve to substantially limit the intermetallic interaction to one 82% σ in character.

$Cp(CO)Mo(\mu\text{-}CO)_2Rh(PH_3)_2$ (IV) appears to be most similar, from the metal–metal bonding standpoint, to binuclear 9 (9′) in view of its short Mo–Rh distance (2.588 Å) which nears the sum of covalent radii (2.55 Å). In valence bond terms, the intermetallic interaction may be convincingly portrayed as a single Mo–Rh bond in combination with a dative (presumably π-type) Rh⩾Mo contribution. Surprisingly, the calculations do not support this depiction. Although a significant interaction does exist, the total overlap population between the metals is substantially lower than those of I and 9′ and the overlap due to the contribution from π-type orbitals is small (23%). In effect, the calculation suggest that despite the existence of what appear to be normal CO bridges, the complex may best be electronically understood by envisioning a Cp-

(73) In order to probe this phenomenon, we varied the Zr–Rh distance in 9′ from 2.20 to 3.00 Å. Across this range the π-overlap drops in a linear fashion from 0.448 to 0.160; the σ-overlap starts at 0.286, crests at 0.306 (2.45–2.55 Å), and drops to 0.262.

(74) (a) Burdett, J. K. *J. Chem. Soc., Dalton Trans.* **1977**, 423–428. (b) Pinhas, A. R.; Hoffmann, R. *Inorg. Chem.* **1979**, *18*, 654–658. (c) Summerville, R. H.; Hoffmann, R. *J. Am. Chem. Soc.* **1979**, *101*, 3821–3831.

(75) Lubben, T. V.; Wolczanski, P. T. *J. Am. Chem. Soc.* **1987**, *109*, 424–435.

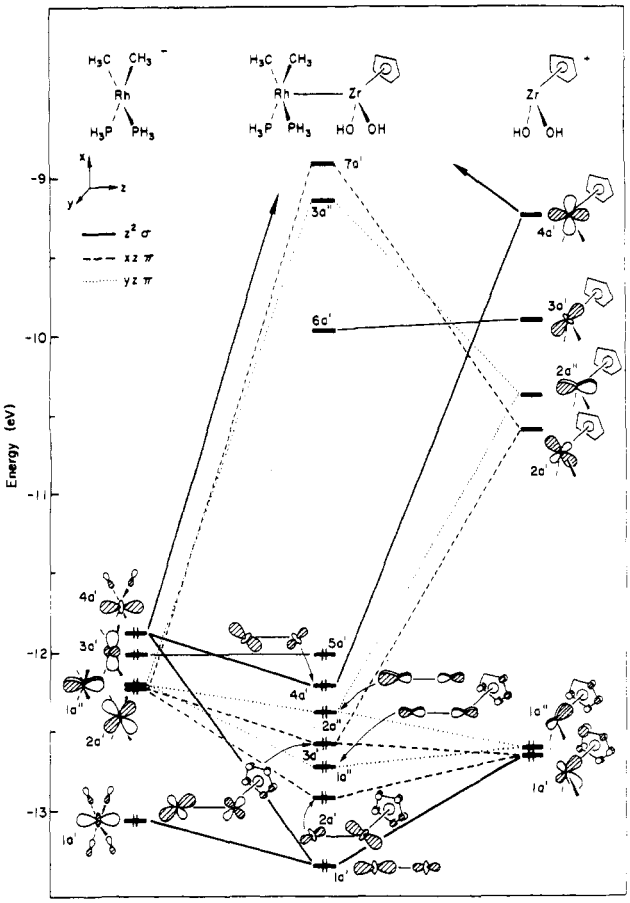

Figure 6. Molecular orbital diagram of $Cp(HO)_2Zr$–$Rh(PH_3)_2Me_2$ (**9'**), the model for **9**.

$(CO)_3Mo^-$ unit σ-donating to the $(Ph_3P)_2Rh^+$ fragment. The latter prefers to donate electron density not to the formally 16e (in IV) Mo center but to the carbonyl ligands in forming the strong bridges. Additional back-donation from Rh to Mo is a secondary contribution; thus the tight intermetallic interaction is driven mostly by bridge formation. Indeed, it is apparent from even these limited examples that bridging units tend to dominate the energetics of binuclear systems, relegating the metal–metal interactions to secondary roles.[74]

From the chart in Figure 5, it is clear that only **9'** possesses a substantial π-interaction, greater than 50% of the total overlap between the disparate metals. A review of the X-ray structural investigation of **9** and the calculation with resulting molecular orbital diagram in Figure 6 highlight several features critical to the formation of a strong intermetallic interaction: (1) the lack of direct bridges akin to μ-PR_2 or μ-CO units necessitates the bonding to be M–M' in origin, unlike II–IV; (2) the μ-OCH_2Ph_2P bridges have proven to be quite flexible, allowing the Rh and Zr to approach one another, thereby engendering substantial π-overlap; (3) the Zr is d^0, minimizing detrimental electron–electron repulsions in addition to providing appropriate empty $d\pi$ and $d\sigma$ orbitals for bonding; (4) the Zr center ($CpZr(OH)_2^+$) is electron-deficient (14e, assuming the OH(R) groups contribute a maximum of 3e) and therefore the empty $d\sigma$ and $d\pi$ orbitals are energetically available to strongly interact with the Rh; (5) the Rh/Zr alignment is such that the d_{z^2} of the square-planar Rh unit is directed toward an empty three-legged piano stool site on Zr, while the d_{xz} and d_{yz} are similarly pointed toward Zr π-type orbitals; and (6) the greater radial extension of 4d orbitals provides for stronger M–M' interactions in the case of second-row metals.

Considering the complexity of the diagram in Figure 6, an overview of the Rh/Zr orbital interactions is appropriate. One aspect of the bonding depicted by the MO scheme concerns the tremendous disparity in energies between orbitals of the electropositive Zr and relatively electronegative Rh centers.[72] The scheme thereby supports the donor/acceptor view in which the bimetallic may be broken into a square-planar, anionic $[P_2RhMe_2]^-$ unit bonded to $[Cp^*Zr(OR)_2]^+$. A complication resulting from these energy differences can be seen in the unfavorable mixing of the Cp–Zr bonding orbitals with the Rh–Zr combinations. For example, MO's 1a'' (Rh–Zr op = 0.03) and 2a'' (Rh–Zr op = 0.08), which describe the π-bonding in the *yz* plane, do not contribute significantly to the overall π-bonding in the complex. The situation is analogous to the three-orbital mixing in allyl; 1a'' is a strong CpZr bonding combination, 2a'' has very little electron density on Zr, and 3a'' is the antibonding MO. While the unfavorable admixing of Cp orbitals plays a role in all of the remaining Rh–Zr orbitals, the a' combinations are not as significantly affected as the a''. Neglecting this complication for simplicity, the Rh–Zr bonding denoted by the 1a', 2a', and 3a' orbitals provides the majority of the overlap crucial to the formation of a strong heterometallic bond. Due to the low symmetry, the mixing of orbitals leads to some ambiguity when classifying the type of interaction present. For example, 1a' describes a d_{z^2}–d_{z^2} σ-orbital (op = 0.120), but 2a' has both σ- and π-components (op 0.133) while 3a' is virtually all π in character (op 0.119). The remaining two occupied orbitals contribute little to the Rh–Zr bond: 4a' because of the low electron density on Zr and 5a' because of its δ-character. To summarize the heterobimetallic bond in **9** (**9'**), the σ-component is best thought of as a composite of d_{z^2}–d_{z^2}-type orbitals and the major π-component is d_{xz}–d_{xz} in origin.

Concluding Remarks

The complexes prepared in this study were designed to model heterogeneous surfaces selective toward the synthesis of oxygenates under Fischer–Tropsch conditions.[16-19] In this case, the combination of Zr and Rh is presented as a homogeneous analogue to rhodium on zirconia (Rh/ZrO_2).[16] Although the heterobimetallic species herein will certainly not exhibit the same behavior as an ensemble of $\sim 10^{20}$ of these atoms, a reasonable perspective of the roles the disparate metals play in CO reduction may be attained. From the compounds examined, the interplay between Rh and Zr varies from being limited to one where Zr is a Lewis acidic anchor[29,76] for the bridging acetyl in $Cp^*Zr(\mu\text{-}OCH_2Ph_2P)_2(\mu_2\text{-}\eta^2\text{-}O{=}C(CH_3))(\mu\text{-}Cl)RhCO$ (**4**) to the extreme in $Cp^*Zr(\mu\text{-}OCH_2Ph_2P)_2RhMe_2$ (**9**), where a multiple bond is present. Each may be relevant to the early/late metal interface of a surface under different circumstances.

The mode of μ-acetyl formation during the construction of **4**, as depicted in Scheme I, represents a CO reduction sequence that utilizes both metals, since the bridging C_2-oxygenate is comprised of a Me derived from Zr and a CO from Rh. In stabilizing this fragment, both metals operate in a cooperative fashion; the more electron-rich Rh binds the μ-acetyl through both σ- and π-bonding while Zr functions as a strong oxophile. Spectral studies support this bonding description, depicted by the resonance forms in Figure 1. Since surface studies often rely upon infrared

(76) (a) Ichikawa, M.; Lang, A. J.; Shriver, D. F.; Sachtler, W. M. H. *J. Am. Chem. Soc.* **1985**, *107*, 7216–7218. (b) Horwitz, C. P.; Shriver, D. F. *Ibid.* **1985**, *107*, 8147–8153. (c) Sachtler, W. M. H.; Shriver, D. F.; Hollenberg, W. B.; Lang, A. F. *J. Catal.* **1985**, *92*, 429–431.

spectroscopy, it should be noted that the characteristic μ_2-η^2-O=CMe IR absorption falls within a range sometimes attributed to surface acetates,[77] which have been proposed as intermediates in acetaldehyde formation. Acetyl groups may be readily removed from the surface through protonation, thus acetates present in heterogeneous systems are likely to serve as a reservoir for acetyl groups.

Protonolysis of **4** to give acetyl–hydride **[4H]Cl** ultimately produces H_3CCHO and dichloride **5**, simulating a product-forming step of a heterogeneous process. The reductive elimination of an acetyl–hydride is a common reaction,[33] and the chemistry herein suggests that this cleavage is facile. Sources of protons in a heterogeneous system would include H_{ads}, H_2O, and hydroxylated zirconia.[16] As a consequence of acetaldehyde release, chloride binds to the Zr in order to offset the loss of the oxygen-donor bridge. A surface Zr oxide unit would be compensated in a similar manner via the binding of H_2O, a new carbonyl-containing intermediate or surface hydroxide/oxide functionalities.

The strength of the Rh–Zr interaction in $Cp^*Zr(\mu\text{-}OCH_2Ph_2P)_2RhMe_2$ (**9**) may be related to surface structure in two ways. First, the complex serves to illustrate an extreme case of a strong donor/acceptor bond. Strong metal-support interactions (SMSI) are observed in Rh/ZrO_2 and similar catalyst combinations when encapsulation of the late metal by its oxide support is thought to occur.[9] Often, this condition is depicted as a breakdown of the deposited late metal into discrete aggregates. Interactions such as the donor/acceptor bond in **9** may be responsible for the rearrangement of catalyst components to the SMSI state. Second, the Rh–Zr bond may be formally viewed as a covalent bond between Rh(II) and Zr(III). Composite catalysts containing zirconia have not been considered reducible;[16] hence SMSI involving this support material is thought to occur differently than its readily reduced congener, TiO_2. The strength of the intermetallic bond in **9** suggests that ZrO_2 may indeed be reducible, provided compensation from highly Rh(δ–)–Zr(δ+) polarized bonds is possible.

Experimental Section

General Considerations. All manipulations were carried out by using either glovebox, high vacuum line, or Schlenk line techniques. Hydrocarbon solvents were purified by initial distillation from purple sodium/benzophenone ketyl, followed by vacuum transfer from the same. Small amounts of tetraglyme (2–5 mL/2000 mL) were added to saturated hydrocarbons to solubilize the ketyl. Methylene chloride was twice distilled from P_2O_5. Chloroform was washed with water to remove MeOH, predried over $CaCl_2$, refluxed over fresh $CaCl_2$, and distilled onto new $CaCl_2$ from which it was vacuum transferred for use. All NMR solvents were dried over activated 4-Å sieves prior to use. Cp^*ZrMe_3 (**1**),[21] $[(OC)_2RhCl]_2$ (**3**),[22] $(Ph_3P)_3RhMe$ (**8a**),[38] $(Ph_3P)_3RhH$ (**8b**),[42] and $HOCH_2Ph_2P$[13] were prepared via literature methods. Methyl iodide was dried over CaH_2 and vacuum transferred from the same.

Proton NMR spectra were recorded on a Varian EM-390, XL-200, or XL-400 spectrometer. $^{31}P\{^1H\}$ and $^{13}C\{^1H\}$ NMR spectra were obtained by using a JEOL FX90Q or Varian XL-200 or XL-400 instrument; the former were referenced to an external PCl_3 standard (+219.0 ppm downfield of H_3PO_4) and the latter to an internal solvent peak. Infrared spectra were obtained by using either a Perkin-Elmer 357 or a Mattson FT-IR spectrophotometer. Gas chromatographic studies were conducted by using a Hewlett-Packard 5890 instrument equipped with a capillary column (Me-silicone (procedure 6), cross-linked 5% Ph,Me-silicone (procedure 7)) and flame ionization detector. Analyses were performed by Analytische Laboratorien in West Germany.

Procedures. 1. $Cp^*ZrMe(OCH_2PPh_2)_2$ (2). To a slurry of $HOCH_2PPh_2$ (900 mg, 7.17 mmol) in 10 mL of hexane was added Cp^*ZrMe_3 (**1**, 565 mg, 2.08 mmol). The immediate evolution of methane was noted, and an additional 2-mL portion of hexane was added. The reaction mixture was placed under Ar (1 atm) and the needle valve cracked open for a few seconds to allow small amounts of air to diffuse into the flask. This "partial oxidation" procedure caused the precipitation of white microcrystalline **2** (94% yield, 91% pure). Yields varied from ~85 to 94% with purities of ~85–91%. Anal. Calcd for **2**, $ZrP_2O_2C_{37}H_{42}$: C, 66.14; H, 6.30. Found: C, 65.86; H, 6.22. ^1H NMR (C_6D_6); δ 0.02 (s, CH_3, 3 H), 1.82 (s, Cp*, 15 H), 4.77 (d, CH_2, 4 H, $^2J_{PH}$ = 7.4 Hz), 7.11 (m, Ph, 8 H), 7.53 (m, Ph, 12 H). $^{31}P\{^1H\}$ NMR: δ –11.24. $^{13}C\{^1H\}$ NMR: δ 10.59 (Cp*), 27.76 (H_3C), 71.47 (d, CH_2, J_{PC} = 9.9 Hz), 118.64 (Cp*), 128.54 (Ph-C(3)), 128.83 (Ph-C(4)), 133.56 (d, Ph-C(2), $^2J_{PC}$ = 17.6 Hz), 137.68 (dd, Ph-C(1), $^1J_{PC}$ = 14.3 Hz, $J_{P'C}$ = 2.2 Hz).

2. $Cp^*Zr(\mu\text{-}OCH_2Ph_2P)_2(\mu_2\text{-}\eta^2\text{-}O{=}C(CH_3))(\mu\text{-}Cl)RhCO$ (4). To a flask containing $Cp^*ZrMe(OCH_2Ph_2P)_2$ (**2**) (659 mg, 0.982 mmol) and $[(OC)_2RhCl]_2$ (**3**, 191 mg, 0.491 mmol) was distilled 10 mL of toluene at –78 °C. Upon warming to 25 °C the starting materials dissolved and the product precipitated as yellow opalescent flakes. Slow bubbling indicated some loss of CO, presumably due to competing pathways (i.e. **5** formation). After ~1 h of stirring, the solution was degassed, ~3 mL of diethyl ether added to aid precipitation, and the solid filtered at –78 °C. After two washes (5 mL and 1 mL) with diethyl ether, the product was dried in vacuo to yield 548 mg of **4** (55%, ~4 mol % impure with **5**). A second crop was ~50% impure with **5**. Yields (45–56%) and purity (amount of **5**) varied from batch to batch. Anal. Calcd for **4**, $RhZrClP_2O_4C_{39}H_{42}$: C, 54.07; H, 4.89; Cl, 4.09. Found: C, 53.86; H, 5.04; Cl, 4.44. ^1H NMR (CD_2Cl_2): δ 1.47 (t, CH_3, 3 H, $^4J_{PH}$ = 1.3 Hz), 2.05 (s, Cp*, 15 H), 4.66 (ddt(v), C*H*H, 2 H, ^2J = 11.4 Hz, $^3J_{RhH} \approx 1$ Hz, J_{PH} = 3 Hz), 5.05 (ddt(v), CH*H*, 2 H, ^2J = 11.4 Hz, $^3J_{RhH} \approx 2$ Hz, $J_{PH} \approx 1$ Hz), 7.39 (m, Ph, 12 H), 7.63 (m, Ph, 8 H). $^{31}P\{^1H\}$ NMR: δ 22.92 (d, J_{RhP} = 149 Hz). $^{13}C\{^1H\}$ NMR: δ 11.44 (Cp*), 40.16 (H_3C), 72.53 (t(v), CH_2, J_{PC} = 18 Hz), 121.58 (Cp*), 128–134 (Ph), 195.18 (CO (**4**–$^{13}C_2$), ddt, J_{RhC} = 52 Hz, J_{CC} = 29 Hz, $^2J_{CP}$ = 15 Hz), 309.22 ($C(CH_3)O$–(**4**–$^{13}C_2$), ddt, J_{RhC} = 30 Hz, $^2J_{CC}$ = 29 Hz, $^2J_{PC}$ = 11 Hz). IR (**4**/**4**-$^{13}C_2$, CD_2Cl_2): ν(CO) 2014/1969 cm^{-1}; $\nu(H_3CC{=}O)$ 1490/1460 cm^{-1}. Conductivity measurements were consistent with a neutral formulation.

3. $Cp^*Zr(\mu\text{-}OCH_2Ph_2P)_2(\mu\text{-}Cl)_2RhCO$ (5). The filtrate from a preparation of **4** (56% isolated yield) was evaporated to leave a solid mixture containing **4** and **5** (~1:1) and byproducts. Into this flask was distilled ~20 mL of $CHCl_3$. The solution was refluxed under argon in the dark for 1.5 h, during which yellow needles appeared at the solvent level and then redissolved. The solvent was removed to leave a foamy solid, to which ~20 mL of diethyl ether was added. Filtration and drying (in vacuo) of the resulting yellow microcrystals gave 323 mg of **5**, with occluded Et_2O and $CHCl_3$. The crude product was ground with a mortar and pestle and dried under dynamic vacuum for 38 h; 186 mg of analytically pure **5** was collected (13% from **3**; i.e. **4** + **5** = 69% total isolated yield). Anal. Calcd for **5**, $RhZrCl_2P_2O_3C_{37}H_{39}$: C, 51.75; H, 4.58; Cl, 8.26. Found: C, 51.49; H, 4.59; Cl, 8.10. ^1H NMR (CD_2Cl_2): δ 2.02 (s, Cp*, 15 H), 5.15 (s, CH_2, 4 H), 7.45 (br s, Ph, 12 H), 7.68 (m, Ph, 8 H). $^{31}P\{^1H\}$ NMR: δ 29.41 (d, J_{RhP} = 122 Hz). IR (Nujol): ν (CO) 1998 cm^{-1}.

4. *trans*-$(HOCH_2Ph_2P)_2Rh(CO)Cl$ (6). To a flask containing $[(OC)_2RhCl]_2$ (981 mg, 0.21 mmol) and $HOCH_2Ph_2P$ (180 mg, 0.833 mmol) was distilled 12 mL of diethyl ether at –78 °C. The mixture was allowed to warm to 25 °C and stirred for ~1 h, incurring precipitation of a pale yellow solid. After removal of 10 mL of Et_2O and replacement with hexane, the solid was filtered and dried under vacuum to yield 203 mg of **6** (81% yield). ^1H NMR (C_6D_6): δ 3.93 (OH, t, ^3J = 7 Hz, 2 H), 4.77 (CH_2, d, ^3J = 7 Hz, 4 H), 6.97 (Ph, mult, 12 H), 7.78 (Ph, mult, 8 H). IR: $\nu(C{\equiv}O)$ 1955 cm^{-1}. Anal. Calcd for $C_{27}H_{26}O_3P_2ClRh$: C, 54.16;

(77) (a) Orita, H.; Naito, S.; Tamaru, K. *J. Catal.* **1984**, *90*, 183–193. (b) Fukushima, T.; Arakawa, H.; Ichikawa, M. *J. Chem. Soc., Chem. Commun.* **1985**, 729–731. (c) Ichikawa, M.; Fukushima, T. *Ibid.* **1985**, 321–323.

H, 4.38. Found: C, 54.03; H, 4.46.

5. Cp*Zr(μ-OCH_2Ph_2P)$_2$(μ-Cl)(μ-I)RhCO (7). To a thick-walled reaction vessel containing **4** (263 mg, 7 mol % **5**; i.e. 0.283 mmol corrected) was distilled 10 mL of CH_2Cl_2 at −78 °C followed by methyl iodide (0.552 mmol, 1.95 equiv), transferred via a gas bulb, at −196 °C. The reaction mixture was stirred at 53–57 °C for ~24 h, after which the volatiles were removed. The resulting yellow solid was filtered from diethyl ether and washed once (2 mL) with the same. Two washes (5 mL each) with hexane and drying in vacuo yielded 207 mg of crude **7** (~84% purity). Recrystallization from toluene/hexane, followed by several washings with hexane and drying under vacuum, provided 182 mg of **7** (4 mol % **5** from starting material, 72% corrected yield). Anal. Calcd for **7**, $IRhZrClP_2O_3C_{37}H_{39}$: C, 46.77; H, 4.14; Cl, 3.73; I, 13.36. Found: C, 46.61; H, 4.27; Cl, 3.63; I, 13.21. ^{1}H NMR (CD_2Cl_2): δ 2.12 (s, Cp*, 15 H), 5.33 (d, C*H*H, 2 H, ^2J = 12 Hz), 5.45 (dt(v), CH*H*, 2 H, ^2J = 12 Hz, J_{PH} = 1.6 Hz), 7.29 (m, Ph, 4 H), 7.51 (m, Ph, 12 H), 7.78 (m, Ph, 4 H). ^{31}P{^{1}H} NMR: δ 23.42 (d, J_{RhP} = 127 Hz). IR (Nujol): ν(CO) 1994 cm^{-1}.

6. HCl + 4: Quantification of CH_3CHO and Identification of [4H]Cl. To a flask containing **4** (50 mg, 0.60 mmol, ~8 mol % **5**) was distilled ~2.5 mL of CH_2Cl_2 at −78 °C. Cyclohexane (0.060 mmol, GC standard) and HCl (0.060 mmol) were condensed in at −196 °C via a gas bulb. The reaction mixture was thawed and stirred at room temperature for ~4 days. The volatiles were then pumped off and collected at −78 °C. This liquid sample was divided into two roughly equal portions and sealed in ampules for GC and GC/MS workup. GC showed 61% (66% if corrected for impurity in starting material) yield of acetaldehyde, which correlated well with the ^{1}H NMR yield of **5** (68% uncorrected). The highest concentration of the observed intermediate **[4H]Cl** occurred ~3.5 h into the reaction (37% of total Cp* integration by ^{1}H NMR). **[4H]Cl**: ^{1}H NMR (CD_2Cl_2) δ −15.21 (dt, RhH, 1 H, J_{RhH} = 28 Hz, J_{PH} = 9 Hz), 1.05 (t, CH_3, 3 H, J_{PH} < 1 Hz), 2.10 (s, Cp*, 15 H), 5.10 (dt(v), C*H*H, 2 H, ^2J = 12 Hz, J_{PH} = 3 Hz), 5.60 (d, CH*H*, 2 H, ^2J = 12 Hz), 7.45 (m, Ph, 12 H), 7.79 (m, Ph, 4 H), 8.02 (m, Ph, 4 H); ^{31}P{^{1}H} NMR δ 14.26 (d, J_{RhP} = 98 Hz); IR (from 4/4-$^{13}C_2$, CD_2Cl_2) ν(CO) 2097/2050 cm^{-1}, ν(H_3CC=O) 1542/1508 cm^{-1}.

7. CH_3I + 4: Quantification of Acetone. To a small glass reaction vessel containing **4** (42 mg, 0.049, 4 mol % impure with **5**) was distilled 2 mL of THF at −78 °C. *n*-Heptane (0.0400 mmol, GC standard) and MeI (0.0901 mmol) were condensed in at −196 °C from a gas bulb. The reaction mixture was stirred at 49–53.5 °C for 20 h, followed by storage at room temperature for 4 days. The volatiles were collected and analyzed by GC (cross-linked 5% Ph,Me-silicone capillary column), which showed 89% (93% if corrected for impurity **5** in starting material) yield of acetone and 0.041 mmol of MeI leftover. A ^{1}H NMR spectrum of the solid residue indicated ~85% (uncorrected) **7** with some occluded MeI.

8. *cis*-Cp*Zr(μ-OCH_2Ph_2P)$_2$RhMe$_2$ (9). To a flask containing Cp*ZrMe(OCH_2Ph_2P)$_2$ (**2**, 300 mg, 0.447 mmol) and $(Ph_3P)_3$RhMe (**8a**, 405 mg, 0.448 mmol) was distilled 17 mL of toluene at −78 °C. The reaction mixture was stirred for 5 min in a −78 °C bath, 20 min in a 0 °C bath, and 1.5 h at 25 °C, during which the solution became golden. The toluene was removed, and the resulting solid triturated three times with 10-mL portions of hexane. The light yellow product was filtered, washed three times with hexane, and dried in vacuo to yield 263 mg of **9** (75%). ^{1}H NMR (C_6D_6): δ 0.63 (Me, m, 6 H), 2.13 (Cp*, s, 15 H), 5.78 (C*H*H, d, J_{HH} = 11 Hz, 2 H), 5.97 (CH*H*, d, J_{HH} = 11 Hz, 2 H), 6.56 (Ph, m, 4 H), 6.71 (Ph, m, 2 H), 7.07 (Ph, m, 8 H), 7.40 (Ph, m, 6 H). ^{31}P{^{1}H} NMR: δ 25.92 (d, J_{RhP} = 103 Hz). ^{13}C{^{1}H} NMR: δ 4.23 (Me, ddd, $J_{t\text{-}PC}$ = 73 Hz, J_{RhC} = 26 Hz, $J_{c\text{-}PC}$ = 10 Hz, tentative), 11.16 (Cp*, s), 84.05 (CH_2, mult, AXX'M), 128.53 (Cp* or Ph, s), 128.68 (Ph, s), 129.33 (Ph, s), 132.40 (Ph, m), 133.30 (Ph, m), 136.78 (Ph, m), 138.47 (Ph, m). M_r: found, 793; calcd, 790. Satisfactory combustion analyses could not be obtained. Estimated impurities of a typical batch based on ^{13}C{^{1}H} and ^{31}P{^{1}H} NMR are <5%, consisting mostly of residual PPh_3.

9. Cp*Zr(μ-OCH_2Ph_2P)$_3$ (10). To a flask containing $HOCH_2Ph_2P$ (266 mg, 1.23 mmol) in 6 mL of hexane was added Cp*ZrMe_3 (**1**, 111 mg, 0.410 mmol) at 25 °C. Immediate and vigorous bubbling was noted. Removal of the hexane yielded a clear, colorless oil. Since ^{1}H NMR indicated quantitative formation of **10**, the complex was not isolated, rather generated in situ prior to use. ^{1}H NMR (C_6D_6): δ 1.87 (Cp*, s, 15 H), 4.74 (CH_2, d, 6 H, $^2J_{PH}$ = 6.6 Hz), 7.1 (Ph, m, 18 H), 7.55 (Ph, m, 12 H).

10. Cp*Zr(μ-OCH_2Ph_2P)$_3$RhMe (11). To a flask containing Cp*Zr(μ-OCH_2Ph_2P)$_3$ (**10**, 0.410 mmol, prepared as in 9), dissolved in 12 mL of toluene, was added $(Ph_3P)_3$RhMe (**8a**, 371 mg, 0.410 mmol) at −78 °C. The reaction mixture was allowed to warm to room temperature and stir for 1.5 h. After replacement of the toluene with hexane, the yellow product was collected via filtration, washed with 3 × 5 mL of hexane, and dried under vacuum to give 328 mg of **11** (impure with ~0.55 equiv of PPh_3). ^{1}H NMR (C_6D_6): δ 0.35 (Me, tdd, $J_{c\text{-}PH}$ = 8, $J_{Rh,t\text{-}PH}$ = 1.5, 5 Hz), 2.33 (Cp*, s, 15 H), 4.04 (*t*-PCH_2, s, 2 H), 4.93 (*c*-PC*H*H, d, J_{HH} = 11 Hz, 2 H), 5.04 (*c*-PCH*H*, d, J_{HH} = 11 Hz, 2 H), 6.80 (Ph, m, 18 H), 7.23 (Ph, m, 6 H), 7.54 (Ph, m, 6 H). ^{31}P{^{1}H} NMR (C_6D_6): δ 30.93 (*t*-PCH_2O, dt, J_{RhP} = 116, J_{PP} = 29 Hz), 38.64 (*c*-PCH_2O, dd, J_{RhP} = 153, J_{PP} = 29 Hz). ^{31}P{^{1}H} NMR indicates that the purity of **11** relative to other P-containing species is 91%.

11. Cp*Zr(μ-OCH_2Ph_2P)$_2$Rh(PPh_3) (12). To a flask containing **2** (222 mg, 0.331 mmol) and $(Ph_3P)_3$RhH·0.3Et_2O (**8b**, 302 mg, 0.331 mmol) was distilled 15 mL of diethyl ether at −78 °C. The cherry red slurry was stirred at −78 °C for 15 min and allowed to warm to room temperature while gas evolution was noted. As the solution warmed, its color became dark burgundy and some yellow solid precipitated. After 4 h of stirring, the Et_2O was exchanged for hexane and the resulting rose-brown solid triturated four times with 10-mL portions of hexane, washed several times with same, and dried under vacuum. ^{1}H NMR indicated 0.7 equiv of PPh_3 remained, so the solid was slurried in 10 mL of hexane for ~1 h, refiltered, washed once (3 mL), and dried under vacuum to give 128 mg of dark yellow **12** (34%, impure with 0.4 equiv of PPh_3). A separate NMR tube reaction indicated that the reaction was nearly quantitative (>90% by ^{31}P{^{1}H} NMR). ^{1}H NMR (C_6D_6): δ 2.00 (Cp*, s, 15 H), 6.30 (C*H*H, d mult, J_{HH} = 11 Hz, 2 H), 6.45 (CH*H*, dt(v), J_{HH} = 11, J_{PH} = 4 Hz, 2 H), 6.6–7.5 (Ph multiplets plus free PPh_3). ^{31}P{^{1}H} NMR: δ 13.25 (OCH_2Ph_2P, dd, J_{RhP} = 213, J_{PP} = 66 Hz), 41.74 (RhPPh_3, dt, J_{RhP} = 176, J_{PP} = 66 Hz).

12. *cis*-Cp*Zr(μ-OCH_2Ph_2P)$_2$RhH$_2$(PPh_3) (13). To a thick-walled glass reaction vessel containing **9** (425 mg, 0.539 mmol) and PPh_3 (141 mg, 0.538 mmol) was distilled 12 mL of benzene at −78 °C. The vessel (30 mL) was cooled to −196 °C, charged with 450 Torr of H_2, and sealed and the reaction mixture warmed to room temperature. The stirred solution immediately became very dark red (the color of **13**), and within ~1 h it had become a somewhat lighter red-orange. After 13.5 h, the reaction mixture was frozen (−196 °C), degassed, and recharged with H_2 (510 Torr). After an additional 7 h, no lightening of the solution had occurred, so the mixture was degassed and the benzene replaced by hexane. The dull yellow solid was filtered, washed four times with hexane (3-mL portions), and dried in vacuo to yield 413 mg of **13** (75%). ^{31}P{^{1}H} and ^{1}H NMR spectra of a separate NMR tube reaction indicated a purity of >95%. Hydrogenation (124 equiv of H_2) of a 50-mg (0.063-mmol) sample of **9** and 17 mg (0.063 mmol) of PPh_3 produced 1.9 equiv of CH_4 (Toepler pump); the crude product mixture was 94% **13** by ^{1}H NMR. ^{1}H NMR (21 °C, C_6D_6): δ −7.10 (RhH, br dd, J = 78, 28 Hz, 2 H), 2.26 (Cp*, s, 15 H), 5.45 (C*H*H, d, J_{HH} = 11 Hz, 2 H), 5.91 (CH*H*, br d, J_{HH} = 11 Hz, 2 H), 6.10 (Ph, m, 4 H), 6.79 (Ph, m, 3 H), 6.99 (Ph, m, 18 H), 7.51 (Ph, m, 10 H). VT ^{1}H NMR (C_7D_8, phenyl as above, Cp* at δ 2.25, the two doublets (δ 5.37, 5.83, ^2J = 11 Hz) due to inequivalent PCH_2 protons are broadened somewhat from 21 to −50 °C) of RhH_2 unit: 21 °C, δ −7.18 (br dd, $J_{t\text{-}PH}$ = 72, J_{Rh} = 28 Hz); at 0 °C, δ −7.12 (v br dt); at −19 °C, δ −7.08 (br d't'd, $J_{t\text{-}PH}$ = 102, $J_{RhH} \approx J_{PH}(PPh_3)$ = 28, $J_{c\text{-}PH}$ = 12 Hz); at −49 °C, δ −7.00 (d't'd as above); at −80 °C, the RhH_2 and PCH_2 are broad and undefined. ^{31}P{^{1}H} NMR: δ 31.56 (Ph_2PCH_2O, br dd (undecoupled), J_{RhP} = 130, $J_{t\text{-}PH}$ = 72 Hz), for [RhPPh_3 + free PPh_3]$_x$; δ 29.40 (x = 1, v br s), −3.64 (x = 3, br s), −5.62 (x = 14, br s). VT ^{31}P{^{1}H} NMR (C_7D_8): at 21 °C, δ 32.20 (PPh_2CH_2O, d, J_{RhP} = 130 Hz), 28.7 (PPh_3, v br s); at 0 °C, δ 32.87 (P'Ph_2CH_2, PPh_2CH_2, apparent dd (br), $J_{RhP,P'}$ = 130, "$J_{PP'}$" = 27 Hz), 30.32 (PPh_3, br d, J_{RhP} = 82 Hz); at −19 °C, ABXM pattern (AB patterns, where A and B are PPh_2CH_2 and P'Ph_2CH_2, respectively, centered at δ 33.04 and 31.44 (32.24 av-

erage) separated by 128 Hz ($J_{RhP,P'}$), and X is a broad PPh_3 resonance at δ 29.67 split by Rh (J_{RhP} = 84 Hz); at −49 °C, same ABXM pattern centered at δ 32.91 (AB), 31.32 (AB) (32.16 average, $J_{RhP,P'}$ = 129 Hz) and 29.53 (X, br d, J_{RhP} = 84 Hz); at −80 °C, same ABXM pattern centered at δ 32.50 (AB), 30.89 (AB) (31.70 average, $J_{RhP,P'}$ = 129 Hz) and 29.31 (X, br d, J_{RhP} = 89 Hz). $^{13}C\{^1H\}$ NMR (C_6D_6): δ 11.85 (Cp*), 84.69 (CH_2, m), 120.24 (Cp*), 127.68–128.49 (Ph), 132.2–132.3 (Ph), 134.15 (PPh_3, d, J_{PC} = 15 Hz), 139.17, 143.76 (ipso Ph, AXX'M), 141.4 (ipso, PPh_3, br). IR (C_6D_6): ν(RhH/RhD) 1747/1258 (br, s) cm^{-1}.

13. NMR Tube Reactions. Five millimeter NMR tubes were sealed onto 14/20 ground glass joints and fitted with needle valve adapters. Samples were loaded into the tubes, freeze–pump–thaw degassed (−196 °C), and sealed with a torch.

a. 13 plus 1.0 Equiv of CH_2=CH_2. Via a gas bulb, ethylene (0.011 mmol) was condensed into an NMR tube containing **13** (11 mg, 0.011 mmol) and 0.35 mL of C_6D_6 at −196 °C. Within 2.5 days the ethylene was consumed, providing **12** and ethane.

b. Cp*Zr(μ-OCH_2Ph_2P)$_2$Rh(μ-C_2H_4)PPh_3 (14) from 13 and Excess CH_2=CH_2. Via a gas bulb, ethylene (0.11 mmol) was condensed into an NMR tube containing **13** (11 mg, 0.011 mmol) and 0.35 mL of C_6D_6 at −196 °C. Within 1.5 h the reaction was complete, giving Cp*Zr(μ-OCH_2Ph_2P)$_2$Rh(η-C_2H_4)PPh_3 (**14**) in near quantitative yield concomitant with ethane. The tube was cracked, the contents were transferred to a flask, and the volatiles were removed. The yellow color darkened and a ^1H NMR of the residual solid indicated that **12** had formed. ^1H NMR (**14**, C_6D_6): δ 1.90 (Cp*, s, 15 H), 2.25 (=C*H*H, dd, J_{HH} = 11, J_{RhH} or J_{PH} = 1.4 Hz, 2 H), 3.04 (=CH*H*, br d, J_{HH} = 11 Hz, 2 H), 6.06 (PC*H*H, d, J_{HH} = 11 Hz, 2 H), 6.31 (PCH*H*, dt, J_{HH} = 11, J_{PH} = 3 Hz, 2 H), 6.84 (Ph, m, 4 H), 6.96 (Ph, m, 3 H), 7.03 (Ph, m, 14 H), ~7.17 (Ph, obscured m, "4" H), 7.39 (Ph, m, 6 H), 7.79 (Ph, m, 4 H); C_2H_6 observed at 0.79 ppm. $^{31}P\{^1H\}$ NMR: δ 15.35 (PPh_2CH_2O, d, J_{RhP} = 177 Hz), −4.86 ([Rh–PPh_3] + free PPh_3], br s). $^{13}C\{^1H\}$ NMR: δ 10.70 (Cp*), 37.83 (η-C_2H_4, dt(v), J_{RhC} = 10, J_{PC} = 6 Hz), 86.16 (PCH_2O, m, AXX'M), 118.92 (Cp*), 128.3–128.9 (Ph), 132.41 (Ph, t(v), J = 6 Hz), 132.70 (Ph, t(v), J = 6 Hz), 138.71 (Ph, t(v), J = 12 Hz), 140.60 (Ph, t(v), J = 16 Hz), broadened signal due to free plus apically bound ethylene at δ 122.9, free PPh_3 resonances also observed.

Single-Crystal X-ray Diffraction Analysis of *cis*-Cp*Zr(μ-OCH_2Ph_2P)$_2$RhMe$_2$ (9). Slow vapor diffusion (−20 °C, 1 atm) of hexane into a toluene solution of **9** over a 2-week period provided a 0.15 × 0.25 × 0.30 mm crystal that was subsequently sealed under N_2 in a thin-walled Lindemann capillary. Precise lattice constants, determined from a least-squares fit of 15 diffractometer-measured 2θ values at 25 °C, were a = 11.734 (1) Å, b = 10.524 (1) Å, c = 15.266 (1) Å, α = 104.15 (1)°, β = 93.92 (2)°, and γ = 112.90 (2)°. The cell volume was 1766.5 (5) Å^3 with a calculated density of 1.485 g/cm^3. The space group was determined to be $P\bar{1}$ and Z = 2. All unique diffraction maxima (h,±k,±l) with $\theta \leq 57°$ were measured on a four-circle, computer-controlled diffractometer with a variable 1° ω scan using graphite-monochromated Cu Kα radiation (1.5418 Å). After correction for Lorentz, polarization, and background, 2717 (60.2%) of the merged and averaged unique data (4510) were judged observed ($|F_o| \geq 3\sigma(F_o)$).[78] Structure solution using heavy-atom techniques and isotropic/anisotropic least-squares refinements proceeded routinely.[79] The Zr and Rh were positioned from the Patterson synthesis, and the non-hydrogen light atoms were revealed by successive Fourier syntheses. At the end of the isotropic refinement (R = 0.124), an empirical absorption correction (μ(Cu Kα) = 74.33 cm^{-1}) was applied (R to 0.074).[80] The minimum, maximum, and average absorption corrections were 0.779, 1.701, and 0.993. Block-diagonal, least-squares refinements (minimization of $\sum w(|F_o| - |F_c|)^2$, where w is based on counting statistics modified by an ignorance factor of p = 0.03) with 44 non-hydrogen atoms, and all hydrogen atoms included at calculated positions have converged to R = 0.063 and a weighted residual (R_w) of 0.051 for the observed reflections. Refinement using all unique data (4510 reflections excluding zeros) resulted in an R of 0.11 and an R_w of 0.095.[81] The fractional coordinates and thermal parameters are listed in Table II.

Table II. Fractional Coordinates and Thermal Parameters[a] for Cp*Zr(μ-OCH_2Ph_2P)$_2$RhMe$_2$ (9)

atom	x	y	z	B(iso), Å^2
Rh	0.3034 (1)	0.1666 (1)	0.2617 (1)	6.1 (1)
Zr	0.2464 (1)	−0.0801 (1)	0.1720 (1)	6.8 (1)
P1	0.4013 (4)	0.1322 (4)	0.3753 (2)	7.1 (2)
P2	0.4723 (4)	0.2353 (4)	0.1907 (3)	7.4 (2)
O1	0.3432 (8)	−0.1234 (9)	0.2586 (5)	8.1 (4)
O2	0.3575 (8)	−0.0304 (8)	0.0847 (5)	7.9 (4)
C1	0.4347 (13)	−0.0302 (15)	0.3310 (8)	7.6 (7)
C2	0.4247 (13)	0.1090 (12)	0.0785 (8)	7.3 (6)
C3	0.1397 (12)	0.1448 (14)	0.3126 (8)	7.8 (7)
C4	0.1999 (14)	0.1766 (16)	0.1525 (9)	9.6 (8)
C5	0.0220 (12)	−0.2672 (13)	0.1735 (8)	7.6 (6)
C6	0.0986 (13)	−0.3423 (14)	0.1567 (8)	7.8 (7)
C7	0.1330 (12)	−0.3381 (14)	0.0775 (8)	7.8 (6)
C8	0.0855 (13)	−0.2581 (15)	0.0459 (9)	8.9 (7)
C9	0.0138 (12)	−0.2113 (14)	0.1011 (9)	8.0 (6)
C10	−0.0525 (14)	−0.2587 (16)	0.2446 (10)	10.2 (8)
C11	0.1287 (15)	−0.4192 (14)	0.2152 (10)	10.4 (8)
C12	0.2131 (14)	−0.4069 (16)	0.0365 (10)	10.9 (8)
C13	0.0960 (15)	−0.2343 (17)	−0.0417 (9)	11.0 (8)
C14	−0.0696 (14)	−0.1412 (16)	0.0856 (11)	10.2 (8)
C15	0.3116 (11)	0.0826 (14)	0.4594 (7)	6.4 (6)
C16	0.3464 (13)	0.1672 (15)	0.5450 (8)	8.0 (7)
C17	0.2670 (16)	0.1310 (17)	0.6028 (9)	10.2 (9)
C18	0.1602 (14)	0.0092 (15)	0.5796 (9)	8.9 (8)
C19	0.1265 (13)	−0.0790 (15)	0.4969 (9)	8.0 (7)
C20	0.2039 (12)	−0.0407 (14)	0.4379 (8)	7.6 (7)
C21	0.5531 (12)	0.2657 (13)	0.4366 (8)	7.3 (6)
C22	0.6401 (13)	0.2323 (14)	0.4764 (9)	8.2 (6)
C23	0.7504 (14)	0.3435 (15)	0.5274 (9)	9.6 (7)
C24	0.7788 (14)	0.4839 (15)	0.5364 (10)	10.5 (8)
C25	0.6959 (14)	0.5194 (15)	0.4952 (11)	10.5 (8)
C26	0.5838 (13)	0.4102 (14)	0.4471 (9)	8.2 (7)
C27	0.5130 (11)	0.4147 (13)	0.1759 (8)	6.9 (6)
C28	0.4619 (13)	0.5055 (16)	0.2266 (9)	9.5 (8)
C29	0.4866 (15)	0.6339 (16)	0.2068 (11)	10.6 (8)
C30	0.5538 (15)	0.6758 (16)	0.1483 (11)	11.3 (9)
C31	0.6006 (15)	0.5895 (16)	0.1016 (10)	10.2 (8)
C32	0.5773 (14)	0.4542 (14)	0.1146 (9)	8.5 (7)
C33	0.6276 (13)	0.2410 (15)	0.2244 (8)	8.1 (7)
C34	0.6480 (13)	0.1182 (15)	0.2012 (11)	9.5 (8)
C35	0.7622 (15)	0.1267 (17)	0.2318 (10)	10.1 (9)
C36	0.8533 (15)	0.2464 (19)	0.2830 (10)	11.2 (10)
C37	0.8318 (15)	0.3698 (18)	0.3078 (10)	10.5 (9)
C38	0.7194 (13)	0.3689 (16)	0.2784 (9)	8.9 (7)

[a] From the anisotropic thermal parameters in the form exp[$-(h^2\beta_{11} + k^2\beta^{22} + l^2\beta_{33} + 2hk\beta_{12} + 2hl\beta_{13} + 2kl\beta_{23})$]; the B(isotropic equivalent)'s are derived: B(iso) = 4.0[V^2 det(β_{ij})]$^{1/3}$.

Extended Hückel Calculations. The extended Hückel calculations were performed with weighted H_{ij}'s[82] and parameters taken from previous work.[32,83] The parameters for Ru were generated by charge iteration on I (5s, 2.08, −9.12 eV; 5p, 2.04, −4.1 eV; 4d, 3.835, −11.18 eV, 0.6624, 0.5782, 1.508).

(78) All crystallographic calculations were done on a PRIME 9950 computer operated by the Cornell Chemistry Computing Facility. Principal programs employed were as follows: FOBS86, by G. Van Duyne, Cornell University, 1986; MULTAN 80 and RANTAN 80, by P. Main, S. E. Hull, L. Lessinger, G. Germain, J. P. Declercq, and M. M. Woolfson, University of York, England, 1980; DIRDIF, by P. T. Beurskens et al., University of Nijmegen, Netherlands, 1981; MITHRIL, by C. J. Gilmore, University of Glasgow, Scotland, 1983; SHELXS, by G. Sheldrick, University of Goettingen, 1986; BLS78A, by K. Hirotsu and E. Arnold, Cornell University, 1980; CRYSTALS, by D. J. Watkin and J. R. Carruthers, Oxford University, 1981; ORTEP, by C. K. Johnson, Oak Ridge National Laboratory, 1970; PLIPLOT, by G. Van Duyne, Cornell University, 1984; TABLES, by G. Van Duyne, Cornell University, 1986.

(79) Cromer, D. T.; Mann, J. B. *Acta Crystallogr., Sect. A: Cryst. Phys., Diffr., Theor. Gen. Crystallogr.* **1968**, *A24*, 321–324.

(80) Walker, N.; Stuart, D. *Acta Crystallogr., Sect. A: Found. Crystallogr.* **1983**, *A39*, 158–166.

(81) $R = \sum||F_o| - |F_c||/(\sum|F_o|)$; $R_w = \{\sum w|F_o| - |F_c|)^2/(\sum w|F_o|^2\}^{1/2}$.

(82) Ammeter, J. H.; Burgi, H.-B.; Thibeault, J. C.; Hoffmann, R. *J. Am. Chem. Soc.* **1978**, *100*, 3686–3692.

(83) Summerville, R. H.; Hoffmann, R. *J. Am. Chem. Soc.* **1976**, *98*, 7240–7254.

Acknowledgment. Support from the donors of the Petroleum Research Fund, administered by the American Chemical Society, and Cornell University is gratefully acknowledged. We thank the ARCO Foundation for a fellowship (G.S.F.) and NIH and NSF Instrumentation Programs for support of the Cornell NMR Facility. Prof. Robert C. Fay is acknowledged for helpful discussions.

Registry No. 1, 81476-64-4; 2, 105900-15-0; 3, 14523-22-9; 4, 105900-16-1; [4H]Cl, 105900-19-4; 5, 105900-17-2; 6, 114995-17-4; 7, 105900-18-3; 8a, 15320-81-7; 8b, 16973-49-2; 9, 114995-18-5; 10, 114995-19-6; 11, 114995-20-9; 12, 114995-21-0; 13, 114995-22-1; 14, 114995-23-2; $HOCH_2PPh_2$, 5958-44-1; CH_3CHO, 75-07-0; $CH_3C(O)CH_3$, 67-64-1; C_2H_4, 74-85-1; C_2H_6, 74-84-0.

Supplementary Material Available: Tables of crystal data, fractional coordinates, isotropic and anisotropic thermal parameters, bond distances, bond angles, and ring centroid calculations pertaining to the X-ray crystallographic study of 9 (9 pages); a listing of observed and calculated structure factors (13 pages). Ordering information is given on any current masthead page.

Electrochemical and Spectroelectrochemical Studies of $(TPP)[Ir(CO)_3]_2$ in Nonaqueous Media

K. M. Kadish,* Y. J. Deng, C.-L. Yao, and J. E. Anderson

Department of Chemistry, University of Houston, Houston, Texas 77204-5641

Received December 9, 1987

A modified method for the synthesis of $(TPP)[Ir(CO)_3]_2$ from $[Ir(CO)_3Cl]_2$ and $(TPP)H_2$ where TPP is the dianion of tetraphenylporphyrin was developed and gives a much higher percent yield. Electrochemical and spectroelectrochemical studies of $(TPP)[Ir(CO)_3]_2$ indicate that this binuclear Ir(I) complex undergoes two reversible reductions at the porphyrin π-ring system. Three irreversible oxidations are observed in benzonitrile containing 0.2 M tetrabutylammonium perchlorate, while in CH_2Cl_2, only two irreversible oxidations are recorded. The first oxidation occurs at one of the two Ir(I) centers of $(TPP)[Ir(CO)_3]_2$ and is followed by a rapid chemical reaction that leads to the generation of $[(TPP)Ir]^+ClO_4^-$ or a solvated form of this species in solution. An overall mechanism for the electrochemical conversion of binuclear $(TPP)[Ir(CO)_3]_2$ to monomeric $[(TPP)Ir]^+ClO_4^-$ and the additional reactions of this species are reported. Comparisons are also made between electrochemical properties of binuclear $(TPP)[Ir(CO)_3]_2$ and the binuclear Rh(I) analogue $(TPP)[Rh(CO)_2]_2$.

Introduction

Rhodium porphyrins have demonstrated their ability to undergo a variety of interesting chemical and electrochemical reactions.[1-8] Similar types of reactions may also occur with iridium porphyrins,[9,10] but detailed comparisons between rhodium and iridium porphrins have, in general, not been possible due to the small amount of data available for the iridium complexes. In this regard, studies of iridium porphyrins have generally been hampered by the fact that the synthesis gives relatively low yields and typically results in formation of several different side products.[11-15] This is in contrast to rhodium porphyrins that are generally synthesized in good yields and in high purity.[16]

Recently, the electrochemistry of a binuclear Rh(I) porphyrin was reported.[17] The one-electron oxidation of $(P)[Rh(CO)_2]_2$ is followed by a metal insertion reaction with the ultimate formation of $[(P)Rh]^+$ in solution. It was not clear if this electrochemically initiated insertion is specific to the oxidized binuclear Rh(I) complex or if other binuclear porphyrins containing metals in the +1 oxidation state might possess the same reactivity. This is examined in this paper which reports the first electrochemistry of a binuclear iridium porphyrin as well as an improved method for the synthesis of $(TPP)[Ir(CO)_3]_2$. Electrochemical and spectroelectrochemical results are coupled with ESR studies to give a self-consistent mechanism for oxidation and reduction of this binuclear compound in nonaqueous media.

Experimental Section

Chemicals. Reagent grade benzonitrile (PhCN) was vacuum distilled from P_2O_5 while spectroscopic grade dichloromethane

(1) Ogoshi, H.; Setsune, J.; Yoshida, Z. *J. Am. Chem. Soc.* **1979**, *99*, 3869.
(2) Wayland, B. B.; Del Rossi, K.; *J. Organomet. Chem.* **1984**, *276*, C27.
(3) Paonessa, R. S.; Thomas, N. C.; Halpern, J. *J. Am. Chem. Soc.* **1985**, *107*, 4333.
(4) van Voorhees, S. L.; Wayland, B. B. *Organometallics* **1985**, *4*, 1887.
(5) Kadish, K. M.; Yao, C.-L.; Anderson, J. E.; Cocolios, P. *Inorg. Chem.* **1985**, *24*, 4515.
(6) Anderson, J. E.; Yao, C.-L.; Kadish, K. M. *J. Am. Chem. Soc.* **1987**, *109*, 1106.
(7) Anderson, J. E.; Yao, C.-L.; Kadish, K. M. *Organometallics* **1987**, *6*, 706.
(8) Hughes, R. P. *Comprehensive Organometallic Chemistry*; Wilkinson, G., Ed.; Pergamon: New York, 1982; Vol. 5, p 388.
(9) van Baar, J. F.; van Veen, J. A. R.; Dewit, N. *Electrochim. Acta* **1982**, *27*, 57.
(10) Farbis, M. D.; Woods, B. A.; Wayland, B. B. *J. Am. Chem. Soc.* **1986**, *108*, 3659.
(11) Fleischer, E. B.; Sadasivan, N. *Chem. Commun.* **1967**, *22*, 159.
(12) Sadasivan, N.; Fleischer, E. B. *J. Inorg. Nucl. Chem.* **1968**, *30*, 591.
(13) Sugimoto, H.; Ueda, N.; Mori, M. *J. Chem. Soc. Dalton Trans.* **1982**, 1611.
(14) Cornillon, J.-L.; Anderson, J. E.; Swistak, C.; Kadish, K. M. *J. Am. Chem. Soc.* **1986**, *108*, 7633.
(15) Ogoshi, H.; Setsune, J.; Yoshida, Z. *J. Organomet. Chem.* **1978**, *159*, 317.
(16) Fleischer, E. B.; Dixon, F. L.; Florida, R. *Inorg. Nucl. Chem. Lett.* **1973**, *9*, 1303.
(17) Yao, C.-L.; Anderson, J. E.; Kadish, K. M. *Inorg. Chem.* **1987**, *26*, 2725.
(18) Yoshida, Z.; Ogoshi, H.; Omura, R.; Watanabe, E.; Kurosaki, T. *Tetrahedron Lett.* **1972**, 1077.

0276-7333/88/2307-1979$01.50/0